Chapter 8

Studies on Structural and Mechanical Characterization of Fe-Al_2O_3-ZrO_2 Hybrid Metal Matrix Nanocomposites

Chapter 8
Studies on Structural and Mechanical Characterization of Fe-Al_2O_3-ZrO_2 Hybrid Metal Matrix Nanocomposites

In Chapter 5 and 6 results of extensive investigation on structural and mechanical characterization of Fe - Al_2O_3 metal matrix composites have been reported. It has been observed that formation of nano-structured iron aluminate phase during sintering have strong influence on their hardness, wear, compression and corrosion behavior. These characteristics depend on the content of iron aluminate phase which in turn depend on the concentration of Al_2O_3 and processing parameters. In a similar study done in our laboratory on Fe-ZrO_2 metal matrix nanocomposite it has been found that the structural and mechanical behavior not only depends on the content of ZrO_2, but also on the formation of iron zirconate phase during reactive sintering [Jha et al. (2013)].

These studies indicated that studies on hybrid metal matrix composite containing both Al_2O_3 and ZrO_2 will be of importance. We have selected 5% ceramic reinforcement + 95% Fe (metal) composition of metal matrix nanocomposites and tried to use different fractions of Al_2O_3 with ZrO_2 in it. We prepared two compositions of ZrO_2-Al_2O_3-Fe hybrid metal matrix nanocomposites namely (i) 2.5% ZrO_2- 2.5% Al_2O_3 + 95% Fe (wt%) and (ii) 3.5% ZrO_2 - 1.5% Al_2O_3- 95% Fe (wt%) of hybrid metal matrix nanocomposites. The present chapter discusses the structural and mechanical characterization of Fe-Al_2O_3-ZrO_2 Hybrid Metal Matrix Nanocomposites synthesized via powder metallurgy technique. Characterizations of the fabricated composite specimens include XRD, SEM, Density, Hardness and Wear. Specimens of 2.5% ZrO_2- 2.5% Al_2O_3 composite system have also been characterized with energy dispersive analysis by X-ray. These results indicate that these hybrid composites have superior hardness and wear characteristics than their counter parts. Composite selected for these investigations were prepared by powder metallurgy solid state

sintering route. Mixed and ball milled powders of constituent raw materials and binder dextrin were compacted at a constant load of 7 tons in a cylindrical die followed by sintering in an inert argon atmosphere in the temperature range of 900 - 1100°C for 1 - 3 hour respectively as described in Chapter 4. The detailed nomenclature of the specimens sintered at different temperature and time of hybrid metal matrix nanocomposites systems (i) 2.5% ZrO_2- 2.5% Al_2O_3+ 95% Fe and (ii) 3.5% ZrO_2 - 1.5% Al_2O_3- 95% Fe are given in Table 8.1 and Table 8.2 respectively.

Table 8.1 Nomenclature of the 2.5Zr2.5AFe Hybrid Metal Matrix Nanocomposites

S. No.	Sintering Temperature (°C)	Sintering Time (hour)	Specimen Code
1.	900	1	2.5Zr2.5AFe900(1)
2.	900	2	2.5Zr2.5AFe900(2)
3.	900	3	2.5Zr2.5AFe900(3)
4.	1000	1	2.5Zr2.5AFe1000(1)
5.	1000	2	2.5Zr2.5AFe1000(2)
6.	1000	3	2.5Zr2.5AFe1000(3)
7.	1100	1	2.5Zr2.5AFe1100(1)
8.	1100	2	2.5Zr2.5AFe1100(2)
9.	1100	3	2.5Zr2.5AFe1100(3)

Table 8.2 Nomenclature of the 3.5Zr1.5AFe Hybrid Metal Matrix Nanocomposites

S. No.	Sintering Temperature (°C)	Sintering Time (hour)	Specimen Code
1.	900	1	3.5Zr1.5AFe900(1)
2.	900	2	3.5Zr1.5AFe 900(2)
3.	900	3	3.5Zr1.5AFe900(3)
4.	1000	1	3.5Zr1.5AFe 1000(1)
5.	1000	2	3.5Zr1.5AFe 1000(2)
6.	1000	3	3.5Zr1.5AFe1000(3)
7.	1100	1	3.5Zr1.5AFe1100(1)
8.	1100	2	3.5Zr1.5AFe1100(2)
9.	1100	3	3.5Zr1.5AFe1100(3)

8.1 Structural Characterization of 2.5Zr2.5AFe Hybrid Metal Matrix Nanocomposites

8.1.1 X-Ray Diffraction

Fig. 8.1 shows XRD plots of specimen (a) 2.5Zr2.5AFe900(1) (b) 2.5Zr2.5AFe900(2) and (c) 2.5Zr2.5AFe900(3). All the identified peaks were matched with the JCPDS data file. It was found from the matching that specimen 2.5Zr2.5AFe900(1) and 2.5Zr2.5AFe900(2) showed the presence of iron (Fe), aluminium oxide (Al_2O_3) and iron zirconium oxide (Zr_6Fe_3O) phases respectively. However, specimen 2.5Zr2.5AFe900(3) showed the presence of iron and iron zirconium oxide phases. The iron zirconium oxide phase in the present case is formed due to the reactive sintering between the iron and zirconium oxide particles.

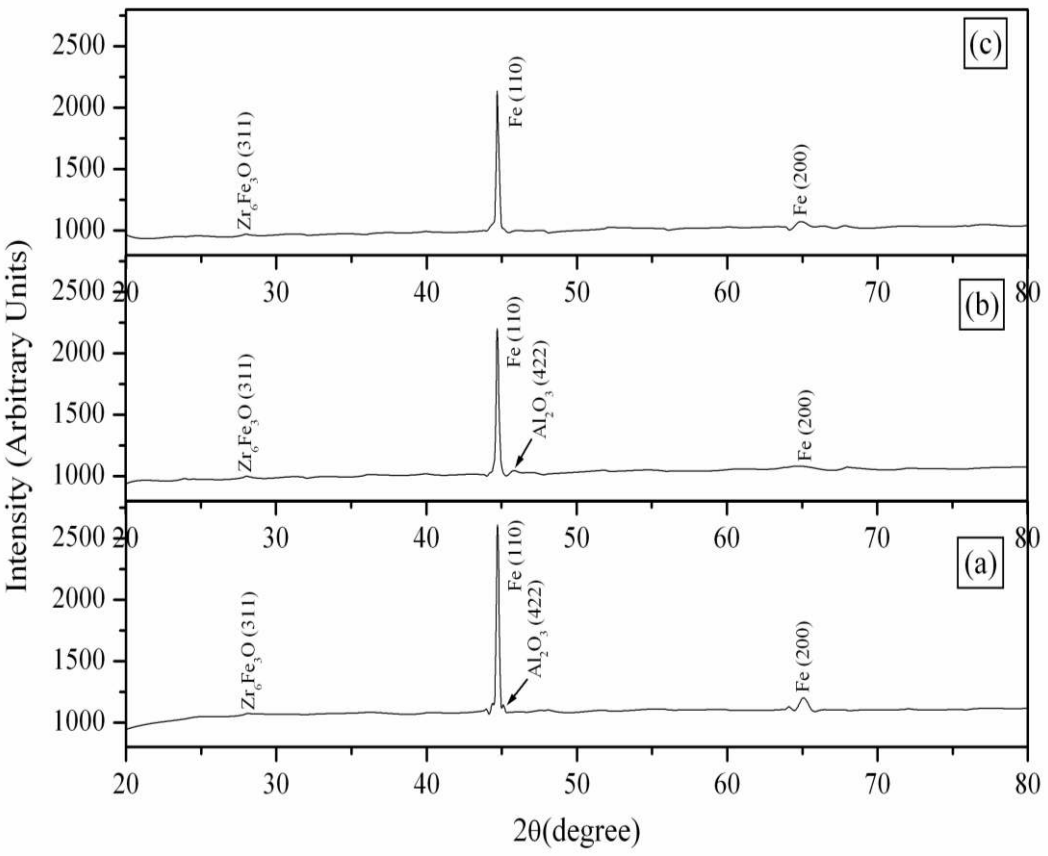

Fig. 8.1 XRD plots of specimens (a) 2.5Zr2.5AFe900(1) (b) 2.5Zr2.5AFe900(2) and (c) 2.5Zr2.5AFe900(3)

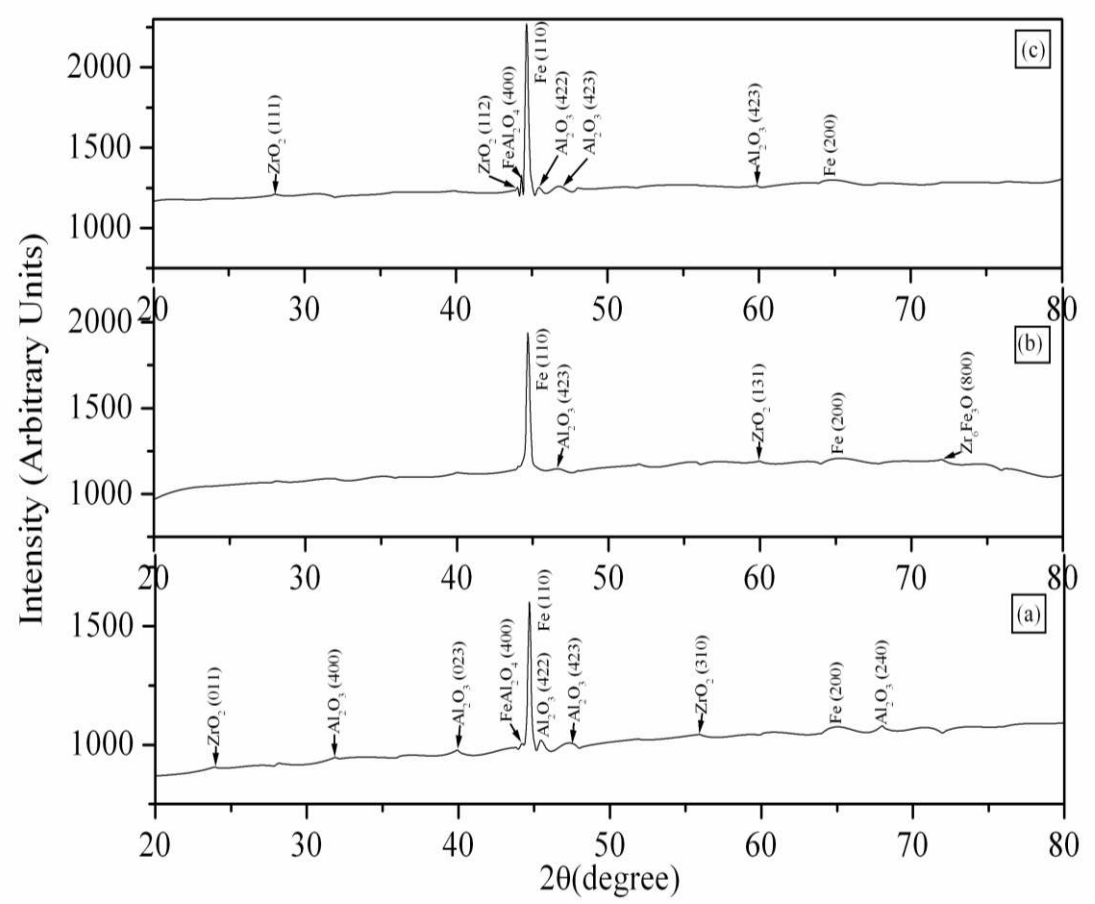

Fig. 8.2 XRD plots of specimens (a) 2.5Zr2.5AFe1000(1) (b) 2.5Zr2.5AFe1000(2) and (c) 2.5Zr2.5AFe1000(3)

Fig. 8.2 shows the X-ray diffraction plots of the specimens 2.5Zr2.5AFe1000(1), 2.5Zr2.5AFe1000(2) and 2.5Zr2.5AFe1000(3) sintered at 1000°C for 1, 2 and 3 hours respectively. All the identified peaks were matched with the JCPDS data file. Specimen 2.5Zr2.5AFe1000(1) shows the presence of peaks of iron (Fe), aluminium oxide (Al_2O_3) and zirconium dioxide (ZrO_2) along with the presence of some traces of iron aluminate ($FeAl_2O_4$) phase respectively. In the similar manner, specimen 2.5Zr2.5AFe1000(2) showed the presence of Fe, Al_2O_3 and ZrO_2 along with the presence of some trace amount Zr_6Fe_3O phase. Again the specimen which was sintered at 1000°C for 3 hour i.e. 2.5Zr2.5AFe1000(3) shows the presence of Fe, Al_2O_3 and ZrO_2 along with the presence of some trace amount of iron aluminate ($FeAl_2O_4$) phase. From the XRD patterns of the specimens it can be attributed that due to the reactive sintering process, an iron aluminate ($FeAl_2O_4$) forms due to the

reactive sintering between iron and aluminium oxide particles and iron zirconium oxide (Zr_6Fe_3O) phase forms due to the reactive sintering between the iron and zirconium dioxide particles respectively.

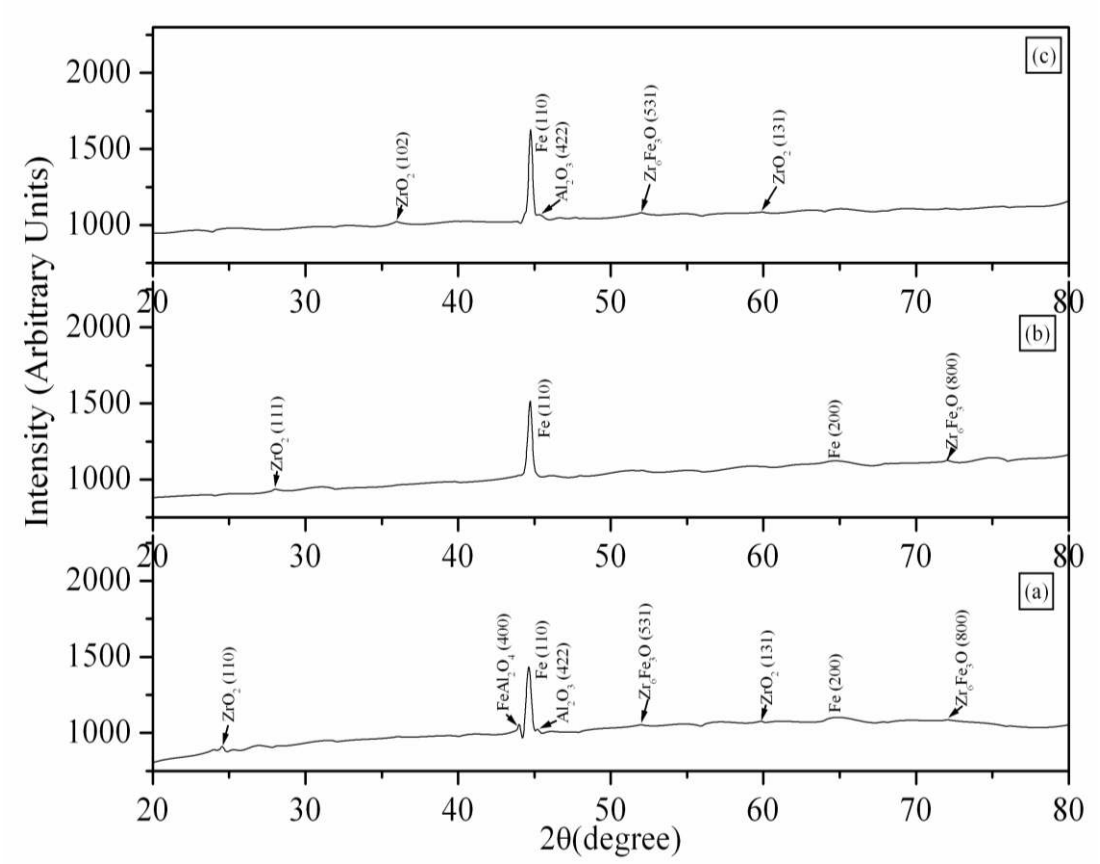

Fig. 8.3 XRD plots of specimens (a) 2.5Zr2.5AFe1100(1) (b) 2.5Zr2.5AFe1100(2) and (c) 2.5Zr2.5AFe1100(3)

Fig. 8.3 illustrates X-ray diffraction plots of the specimens sintered at 1100°C for different time intervals i.e. 2.5Zr2.5AFe1100(1), 2.5Zr2.5AFe1100(2) and 2.5Zr2.5AFe1100(3). Specimen 2.5Zr2.5AFe1100(1) depicts the presence of Fe, Al_2O_3 and ZrO_2 phases along with the presence of trace amount of iron aluminate ($FeAl_2O_4$) and iron zirconium oxide (Zr_6Fe_3O) phases. In the similar manner specimen 2.5Zr2.5AFe1100(2) shows the presence of iron and zirconium dioxide only. In the next spate the specimens 2.5Zr2.5AFe1100(3) show the presence of Fe, Al_2O_3 and ZrO_2 phases along with the presence of trace amount of iron zirconium oxide (Zr_6Fe_3O) phases respectively. On the basis of the above discussion it can be concluded that due to the reactive sintering process, the iron aluminate and iron

zirconium oxide phases forms. At a sintering temperature of 1000°C for 1, 2 and 3 hrs it was seen that iron aluminate phase formation was more in comparison to the iron zirconium oxide phase formation. At 1100°C for different time interval, the iron zirconium oxide phase formation was high in comparison to the iron aluminate phase.

8.1.2 Scanning Electron Microscopy (As Prepared)

Fig. 8.4 shows the SEM micrograph of specimen 2.5Zr2.5AFe900(1) at (a) 1000X (b) 5000X (c) 10000X and (d) 25000X respectively.

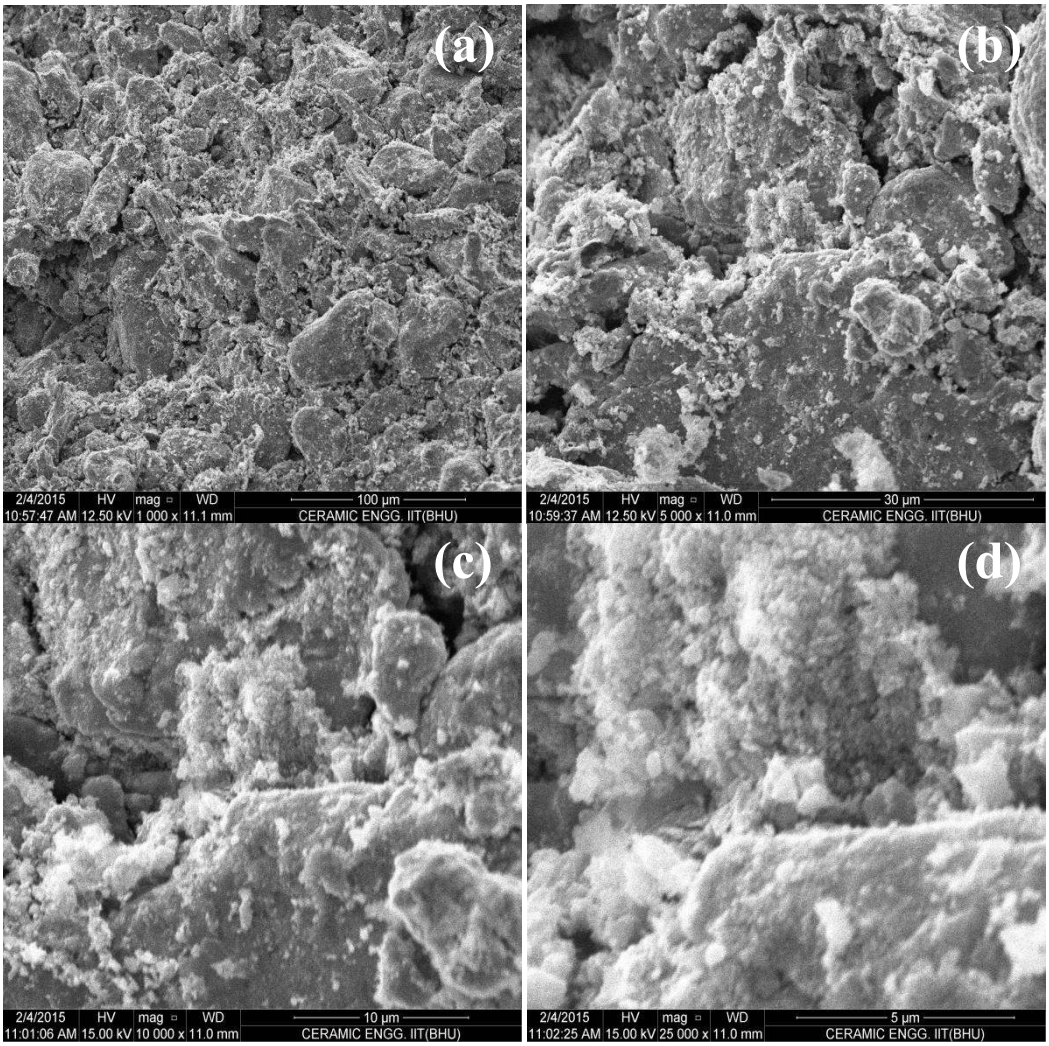

Fig. 8.4 SEM micrograph of specimen 2.5Zr2.5AFe900(1) at (a) 1000X (b) 5000X (c) 10000X and (d) 25000X respectively

Fig. 8.4(a) shows SEM image of the specimen at 1000X illustrating the loosely packed grains of the composite structure. The bonding between the various grains is also small. On increasing the magnification to 5000X [Fig. 8.4(b)] shows the larger size grains of iron with some micrometer size grains of alumina. Some small size alumina grains are sticked on the periphery of large iron grains. Fig. 8.4(c) shows SEM image of the specimen at 10000X illustrating a few sub micron size particles of iron zirconium oxide phase. Lastly Fig. 8.4(d) shows the micrograph of the same specimen at 25,000X illustrating the nano size particle of iron and iron zirconium oxide phase respectively. Low amount of iron zirconium oxide particles can be seen in the present image.

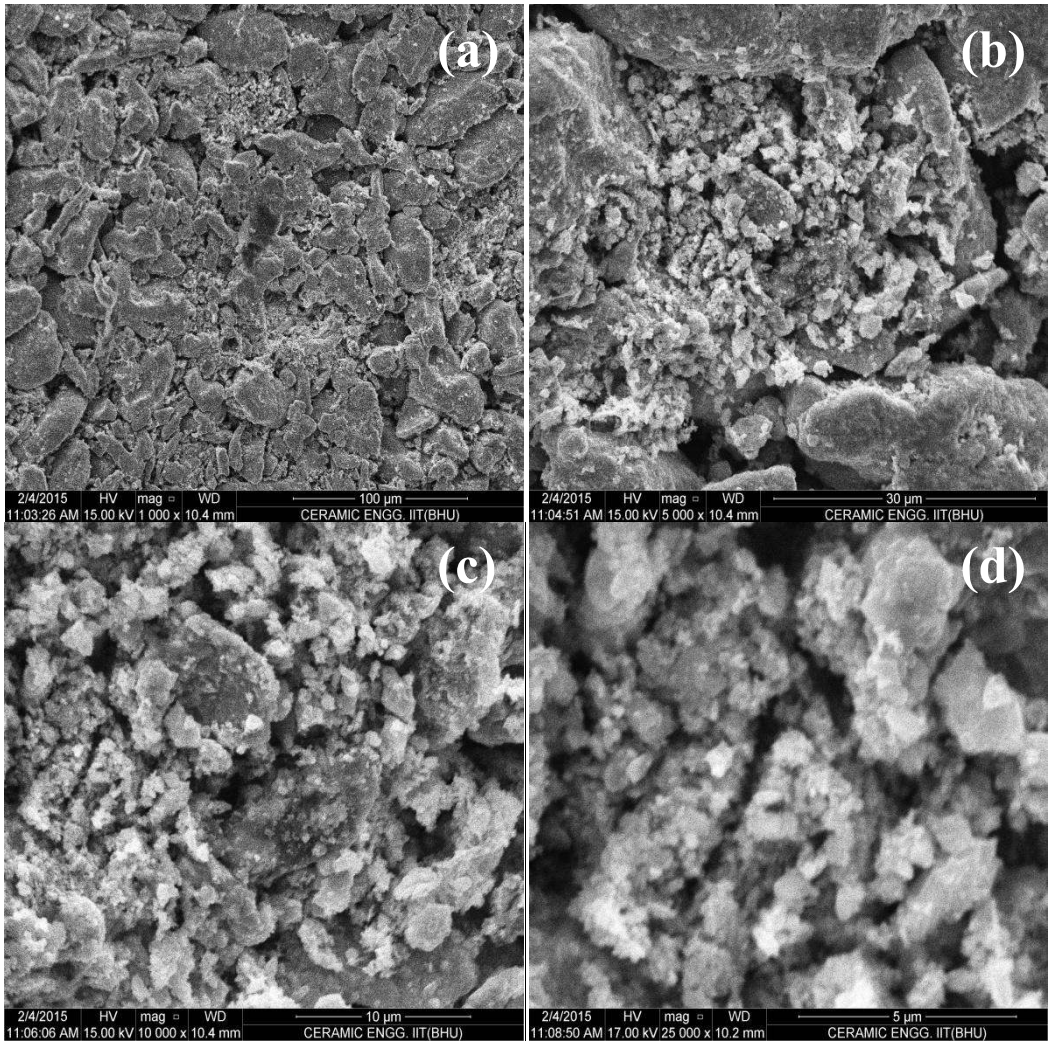

Fig. 8.5 SEM micrograph of specimen 2.5Zr2.5AFe900(2) at (a) 1000X (b) 5000X (c) 10000X and (d) 25000X respectively

Fig. 8.5 shows the SEM micrograph of specimen 2.5Zr2.5AFe900(2) at (a) 1000X (b) 5000X (c) 10000X and (d) 25000X respectively. Fig. 8.5(a) shows the electron micrograph of the specimen at 1000X which illustrates the loosely bound particles of hybrid composites. The densification rate in the present case is high but the density value is less due to which the particle packing factor is reduced. The same specimen when viewed at 5000X shows the grains of iron with the presence of some small amount of alumina particles which gets sticked on the periphery of iron. Fig. 8.5(c) shows the SEM image of the same specimen at 10000X which shows some sub micron size particles of iron zirconium oxide phase.

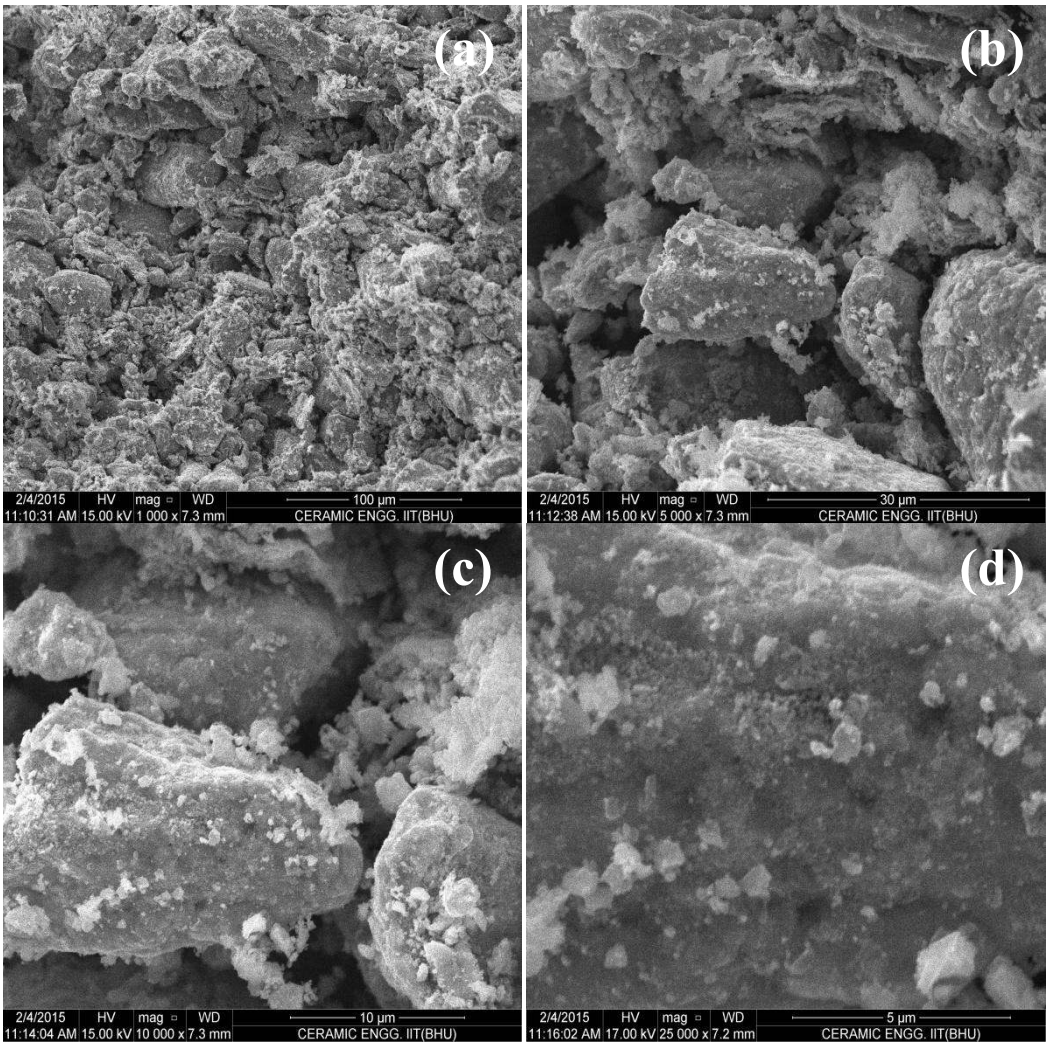

Fig. 8.6 SEM micrograph of specimen 2.5Zr2.5AFe900(3) at (a) 1000X (b) 5000X (c) 10000X and (d) 25000X respectively

Iron zirconium oxide particles are found to be uniformly distributed in the present micrograph. Fig. 8.5(d) shows the electron micrograph of the same specimen at 25000X which shows the presence of nanosize grains of the iron zirconium oxide.

Fig. 8.6 shows the SEM micrograph of specimen 2.5Zr2.5AFe900(3) at (a) 1000X (b) 5000X (c) 10000X and (d) 25000X respectively. Fig. 8.6(a) shows the SEM image of the specimen at 1000X which reveals finer size loose grains of the composite structure. However, due to low temperature but higher time of sintering leads to small amount of densification. Still the present specimen is little bit denser in comparison to the specimen 2.5Zr2.5AFe900(1) and 2.5Zr2.5AFe900(2). Same specimen when viewed at 5000X [Fig. 8.6(b)] shows the larger grains of iron along with the some sub micron size grains of alumina sticked on the periphery of iron grains. Fig. 8.6(c) shows the electron micrograph of the same specimen at 10000X revealing 2-4 μm size grains of iron. Some small grains of iron of size 0.5-1.0 μm are also present. Fig. 8.6(d) shows the scanning electron micrograph of the specimen at 25000X which shows the nano size grains of iron zirconium oxide formed due to the reactive sintering between the iron and zirconia particles. The size of the iron zirconium oxide particles are found to be small in comparison to the specimen 2.5Zr2.5AFe900(1) and 2.5Zr2.5AFe900(2).

Fig. 8.7 illustrates the scanning electron micrograph of the specimen 2.5Zr2.5AFe1000(1) at (a) 1000X (b) 5000X (c) 10000X and (d) 25000X respectively. The micrograph of the specimen at 1000X is shown in Fig. 8.7(a) shows the presence of highly dense phase structure of the hybrid nanocomposite. Amount of the porosity present in the micrograph is almost negligible. In the similar manner Fig. 8.7(b) shows the micrograph of the same specimen at 5000X which shows the separation of the various particles with a clear cut presence of grain boundaries. The grain boundaries present in the micrograph shows the presence of some smaller size particles.

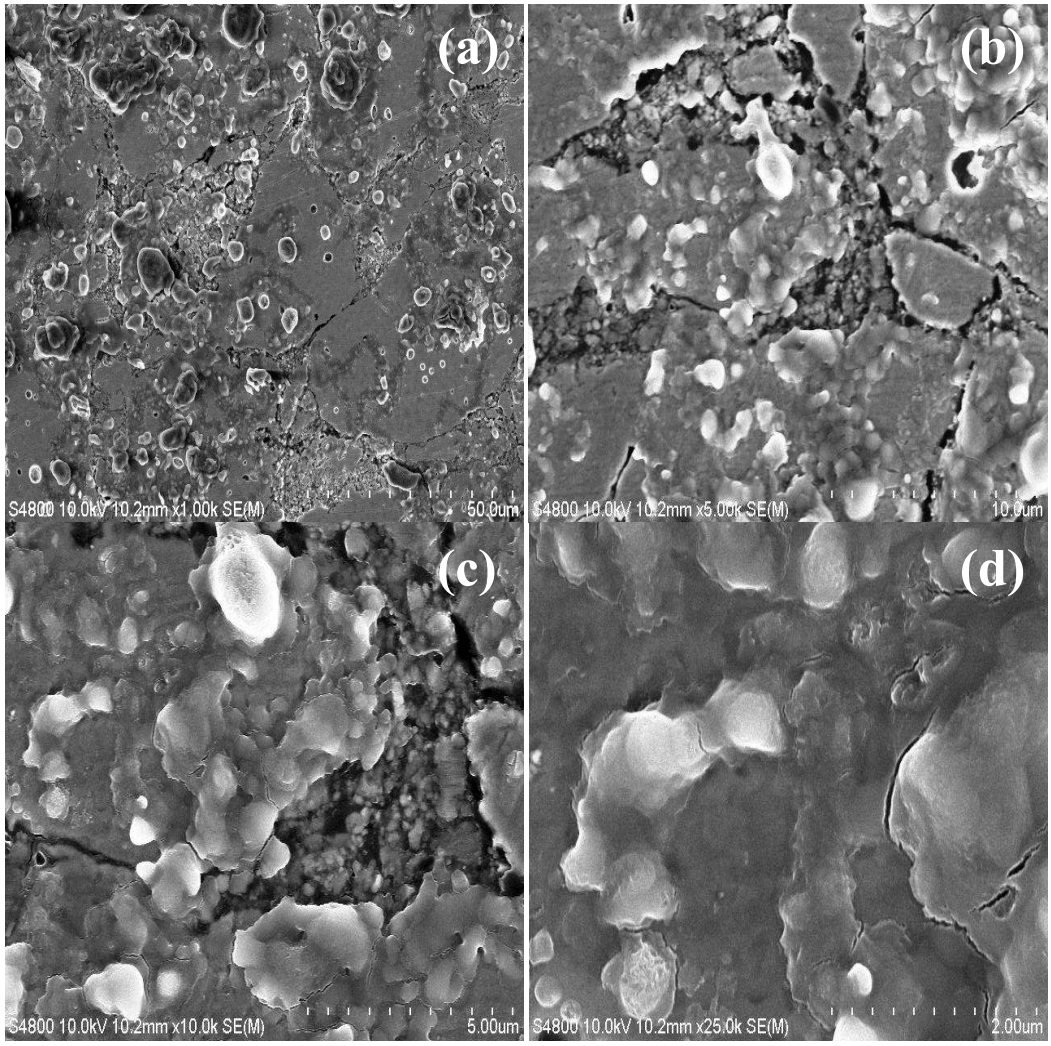

Fig. 8.7 SEM micrograph of specimen 2.5Zr2.5AFe1000(1) at (a) 1000X (b) 5000X (c) 10000X and (d) 25000X respectively

The presence of smaller size particles improves the various properties of the formed nanocomposite system. A clearer view of this nanocomposite system can be seen in the micrograph at 10,000X illustrated in Fig. 8.7(c). The microstructure shows the distributed type grains of various constituents i.e. Fe, Al_2O_3, ZrO_2 and $FeAl_2O_4$. The micrograph of the same specimen is illustrated in Fig. 8.7(d) at 25000X which shows the stable dense nanocomposite structure with better intragranular bonding.

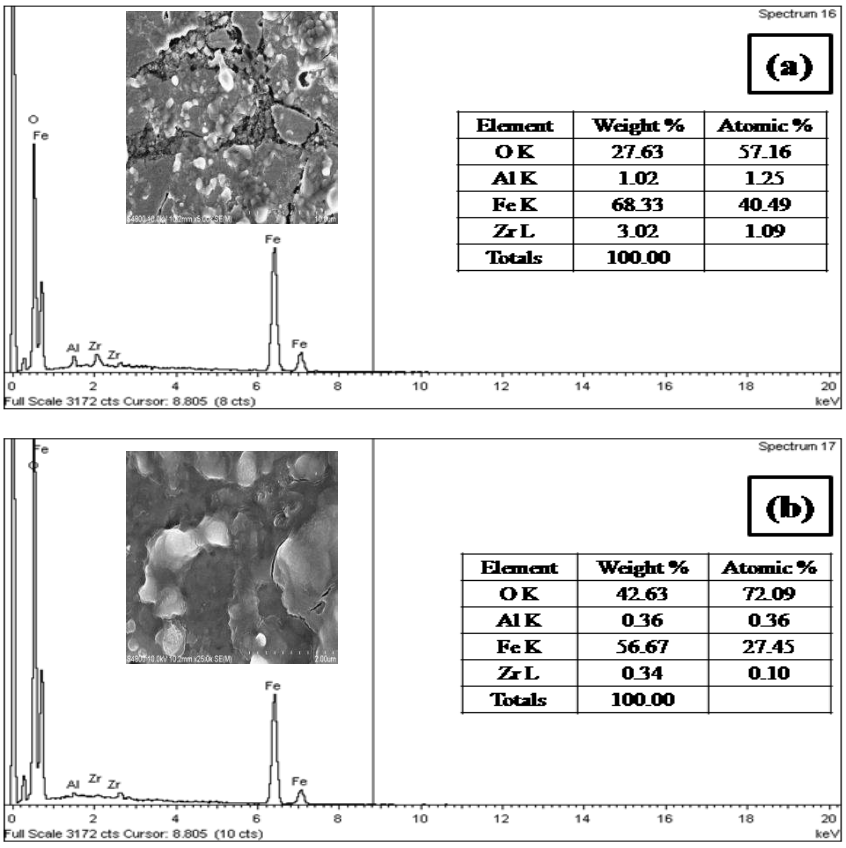

Fig. 8.8 Full Frame EDS and elemental profile of specimen 2.5Zr2.5AFe1000(1) at (a) 5000X and (b) 25000X respectively

XRD patterns reveal the presence of different constituents in the specimen and if the amount of certain phase is small it is not being detected by the instrument. In order to verify the results of XRD studies and to identify the phases microstructurally, EDS studies is done. Therefore, we have characterized the surfaces of hybrid nanocomposite specimen using energy dispersive spectroscopy technique. Full frame EDS of different specimens was carried out for 5000X and 25000X magnification images in this system.

Fig. 8.8 shows the full Frame EDS and elemental profile of specimen 2.5Zr2.5AFe1000(1) at (a) 5000X and (b) 25000X respectively. Full frame EDS of the specimen at 5000X shows the presence of O, Al, Fe and Zr respectively. Oxygen is 27.63 wt%, aluminium is 01.02 wt%, iron is 68.33 wt% and zirconia is 03.02wt%

respectively. Similarly the EDS of the same specimen at 25,000X depicts the presence of oxygen, aluminium, iron and zirconia respectively. Oxygen is 42.63 wt%, aluminium is 00.36 wt%, iron is 56.67 wt% and zirconia is 0.34 wt%. It was found that full frame EDS at 5000X shows more amount of iron, alumina and zirconia in comparison to EDS at 25000X.

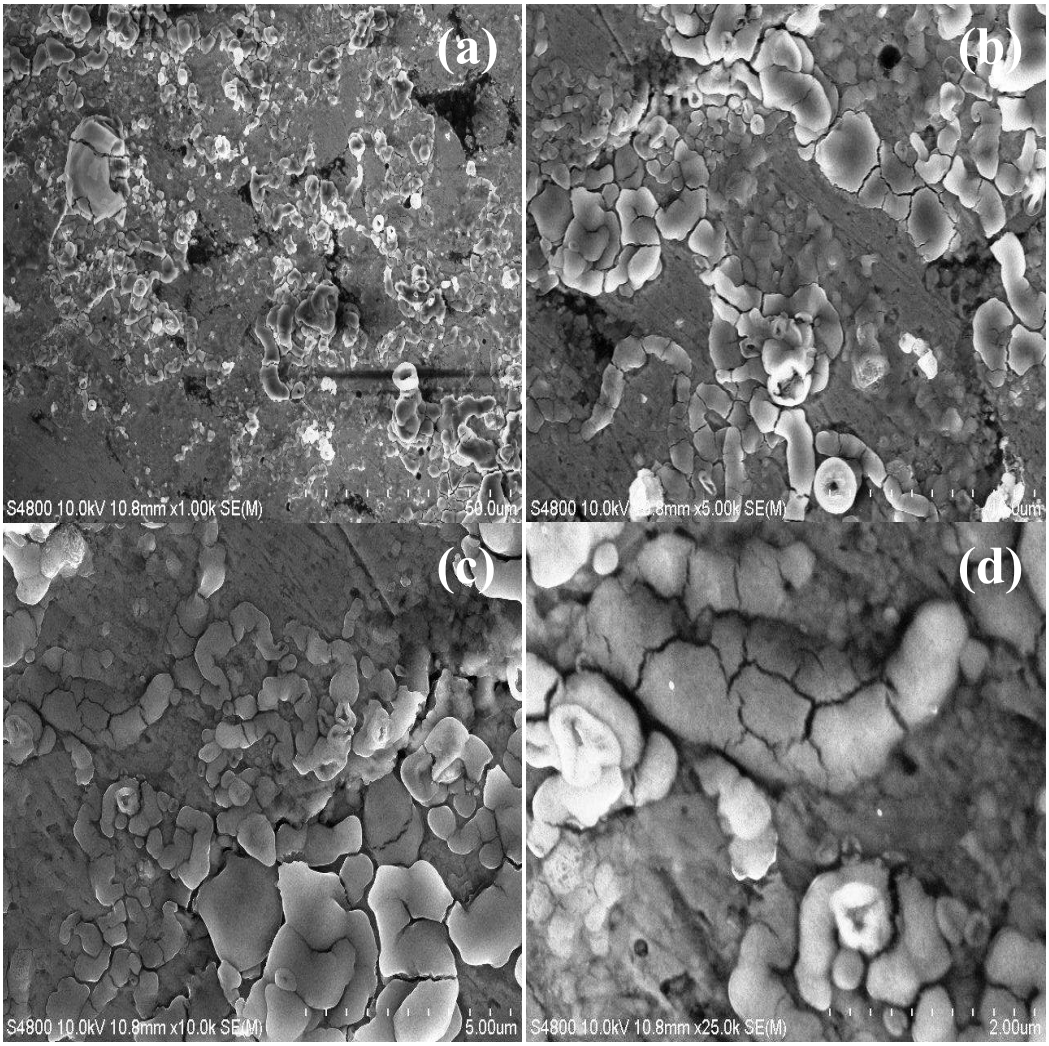

Fig. 8.9 SEM micrograph of specimen 2.5Zr2.5AFe1100(1) at (a) 1000X (b) 5000X (c) 10000X and (d) 25000X respectively

Fig. 8.9 illustrates the SEM micrograph of the specimen 2.5Zr2.5AFe1100(1) at (a) 1000X (b) 5000X (c) 10000X and (d) 25000X respectively. Fig. 8.9(a) shows the micrograph of the specimen at 1000X which describes the highly dense phase

structure of the hybrid nanocomposite. The present micrograph is denser in comparison to the micrograph of the specimen 2.5Zr2.5AFe1000(1). The next micrograph illustrated in fig 8.9(b) at 5000X describes the grains separation with the presence of the grain boundaries. The particles are homogenously distributed in the present system and there is a combination of bigger as well as smaller particles. The same micrograph when viewed at 10000X as illustrated in fig 8.9(c) shows the bigger and smaller size particles of iron. Last micrograph of the same specimen at 25000X (fig 8.9(d)) describes the various particles of Fe, Al_2O_3, ZrO_2 and $FeAl_2O_4$ phases respectively.

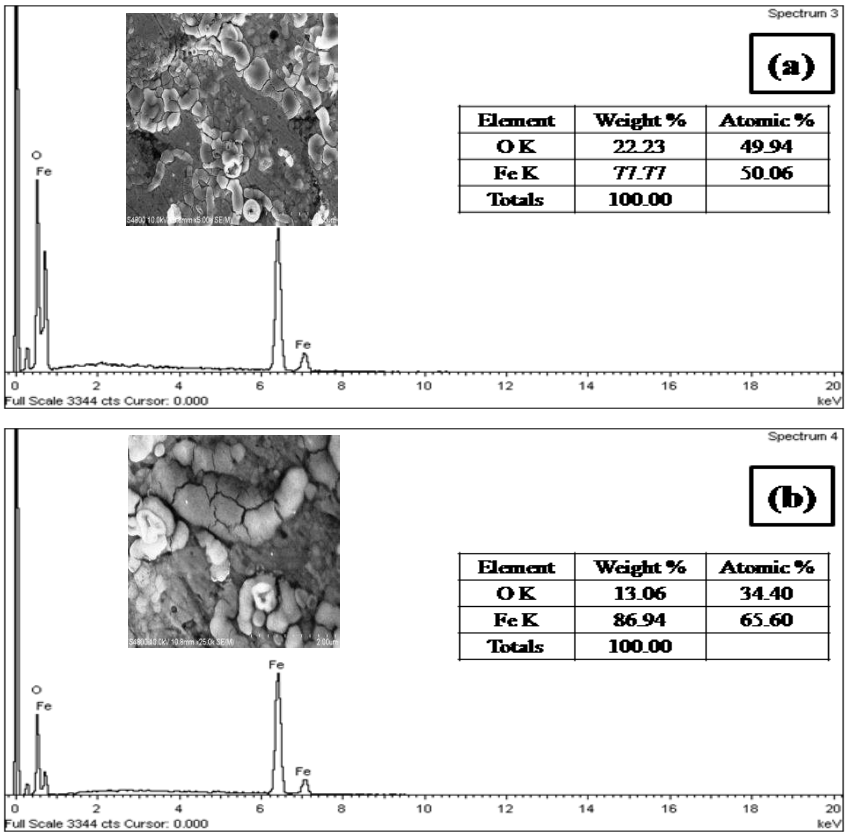

Fig. 8.10 Full Frame EDS and elemental profile of specimen 2.5Zr2.5AFe1100(1) at (a) 5000X and (b) 25000X respectively

Fig. 8.10 shows the full Frame EDS and elemental profile of specimen 2.5Zr2.5AFe1100(1) at (a) 5000X and (b) 25000X respectively. Fig. 8.10(a) describes the full frame EDS of specimen 2.5Zr2.5AFe1100(1) at 5000X which shows the presence of oxygen and iron respectively. Oxygen is 22.23 wt% and iron is 77.77

wt% respectively. Similarly Fig. 8.10(b) describes the full frame EDS of specimen 2.5Zr2.5AFe1100(1) at 25000X which also shows the presence of oxygen and iron respectively. Oxygen is 13.06 wt% and iron is 86.94 wt% respectively. EDS of 5000X magnification shows less amount of iron in comparison to EDS at 25000X magnification. However, amount of oxygen was found to be high in 5000X magnification in comparison to 25000X magnification respectively.

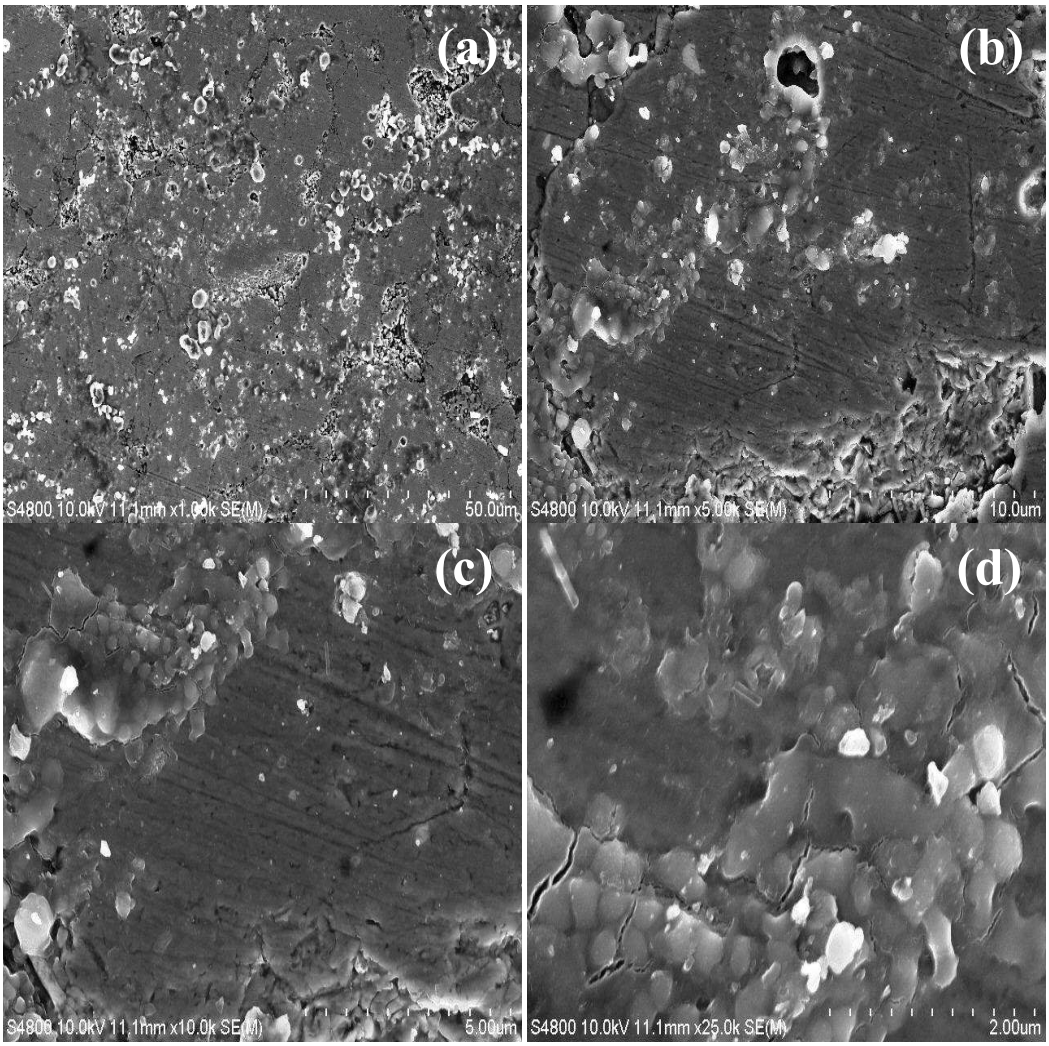

Fig. 8.11 SEM micrograph of specimen 2.5Zr2.5AFe1100(2) at (a) 1000X (b) 5000X (c) 10000X and (d) 25000X respectively

Fig. 8.11 illustrates the SEM micrograph of specimen 2.5Zr2.5AFe1100(2) at (a) 1000X (b) 5000X (c) 10000X and (d) 25000X respectively. Fig. 8.11(a) shows the

electron micrograph of the specimen 2.5Zr2.5AFe1100(2) at 1000X which again shows the dense phase structure with the presence of negligible amount of porosity. The next micrograph at 5000X (fig 8.11(b)) describes some small particles on the outer lining of the structure. The overall system shows some smaller particles which are located on the dense phase structure of the system. The micrographs at 10000X and 25000X illustrated in fig. 8.11(c) and 8.11(d) shows a much well defined system with the presence of particles of Fe, Al_2O_3, ZrO_2 and Zr_6Fe_3O.

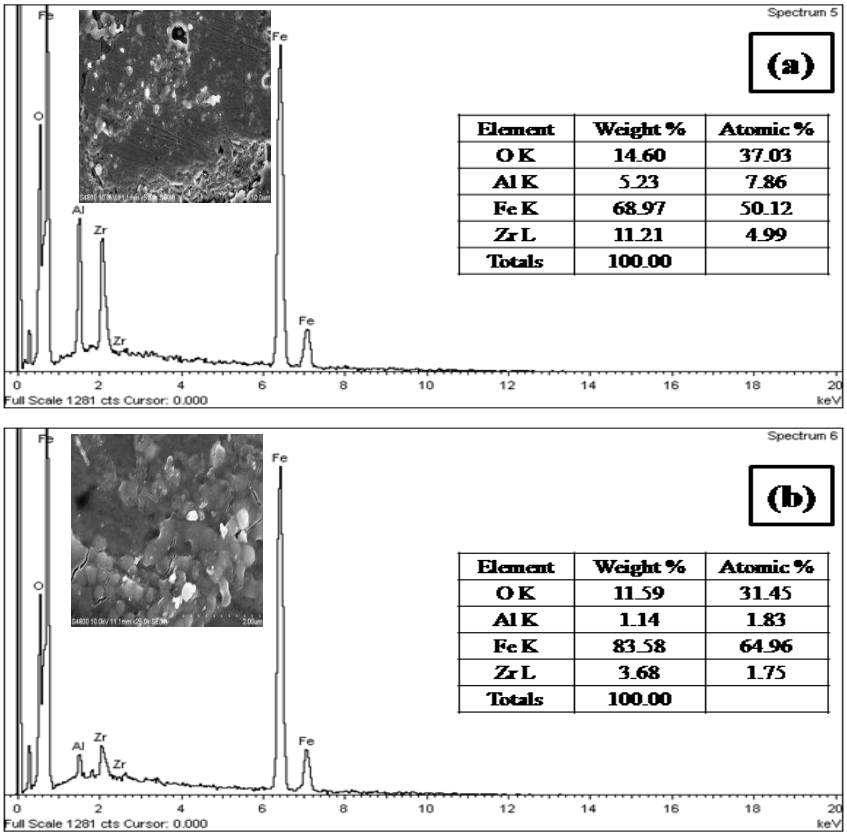

Fig. 8.12 Full Frame EDS and elemental profile of specimen 2.5Zr2.5AFe1100(2) at (a) 5000X and (b) 25000X respectively

Fig. 8.12 shows the Full Frame EDS and elemental profile of specimen 2.5Zr2.5AFe1100(2) at (a) 5000X and (b) 25000X respectively. Fig. 8.12(a) shows the presence of oxygen, aluminium, iron and zirconia respectively. The wt% variations of the constituents were as follows oxygen 14.60%, aluminium 05.23%, iron 68.97% and zirconia 11.23%. Similarly Fig. 8.12(b) illustrated the energy

dispersive spectroscopy of the same specimen at 25000X which again shows the presence of oxygen, aluminium, iron and zirconia respectively. Oxygen was 11.59 wt%, aluminum 01.14 wt%, iron 83.58 wt% and zirconia 03.68 wt% respectively. It can be concluded on the basis of the above discussion that amount of iron was high in the 25000X image as compared to 5000X image. Concentration of alumina, zirconia and oxygen was found to be high in 5000X image as compared to 25000X image.

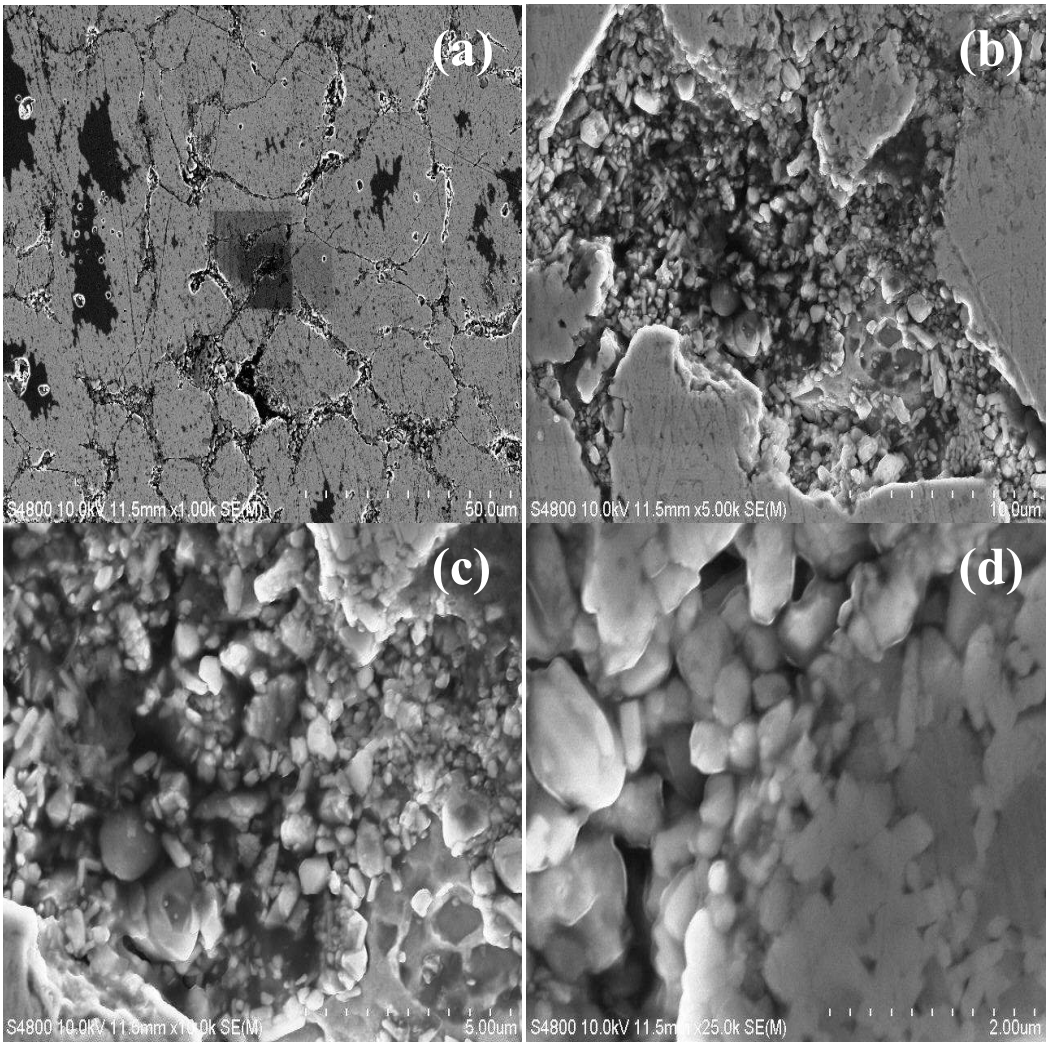

Fig. 8.13 SEM micrograph of specimen 2.5Zr2.5AFe1100(3) at (a) 1000X (b) 5000X (c) 10000X and (d) 25000X respectively

Fig. 8.13 depicts the SEM micrograph of specimen 2.5Zr2.5AFe1100(3) at (a) 1000X (b) 5000X (c) 10000X and (d) 25000X respectively. Fig. 8.13(a) shows the SEM

micrograph of the specimen at 1000X magnification which shows the dense phase structure of the hybrid nanocomposite specimen. The micrograph contains negligible amount of pores. The grain separation with the presence of the grain boundaries can be very easily seen in the present micrograph. In this continuation fig. 8.13(b) shows the electron micrograph of the specimen at 5000X which shows the granulated particles of the constituent phases. The particles in the present micrographs are of the sub micron and micron size.

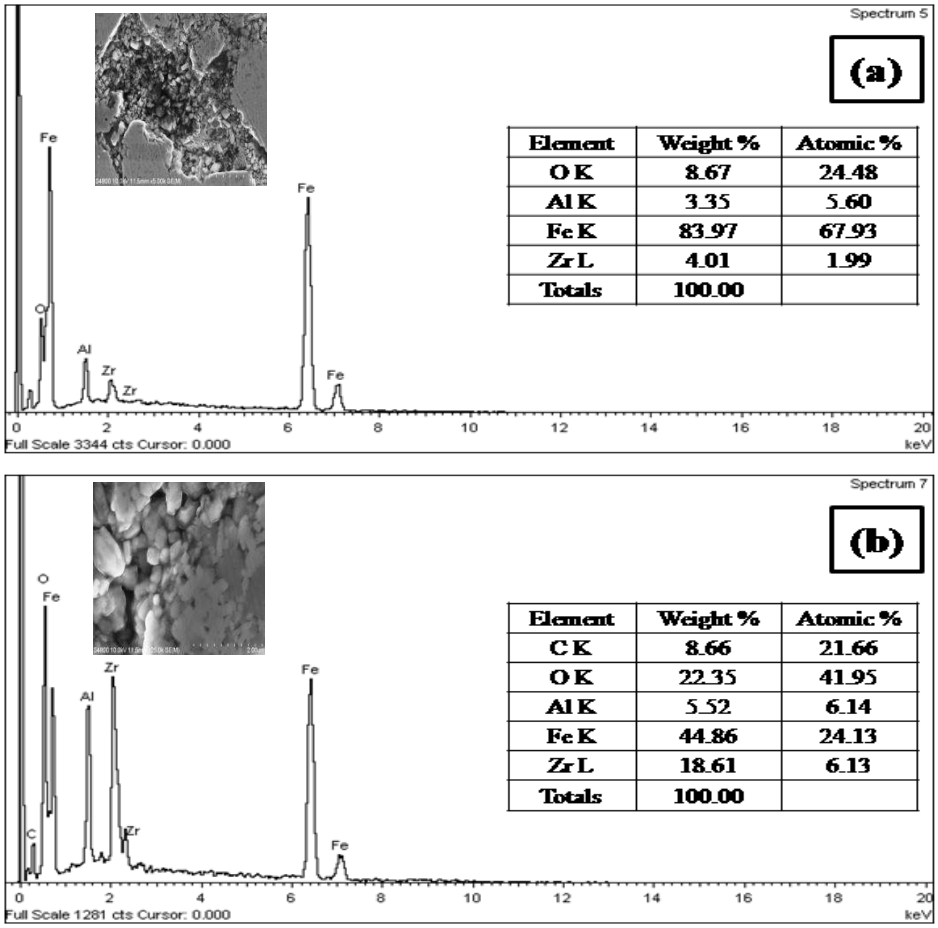

Fig. 8.14 Full Frame EDS and elemental profile of specimen 2.5Zr2.5AFe1100(3) at (a) 5000X and (b) 25000X respectively

The SEM of the same specimen at 10000X is shown in fig 8.13(c) which shows the 2-4 μm size particles of iron, 1-2 μm size particles of Al_2O_3, ZrO_2 and some 0.5-1.0 μm size particles of Zr_6Fe_3O phase. Last micrograph of the same specimen at 25000X is shown in fig 8.13(d) which shows some nano size particles of the Zr_6Fe_3O. It is very

much interesting to note from the electron micrograph that the nano size particles of Zr_6Fe_3O phase increases with the increase in the sintering temperature and time respectively. However, it was also seen that at lower temperature and time of sintering the nano iron aluminate phase forms with only small amount of the iron zirconium oxide phase.

Fig. 8.14 shows the Full Frame EDS and elemental profile of specimen 2.5Zr2.5AFe1100(3) at (a) 5000X and (b) 25000X respectively. Fig. 8.14(a) shows the EDS of the specimen at 5000X which shows the presence of oxygen, aluminium, iron and zirconia phase respectively. Oxygen is 08.67 wt%, aluminium is 03.35 wt%, iron is 83.97 wt% and zirconia is 04.01%. Similarly Fig. 8.14(b) also shows the EDS of the specimen at 25000X which shows the presence of oxygen, aluminium, iron and zirconia phase respectively. Carbon is 08.66 wt%, Oxygen is 22.35 wt%, aluminium is 05.52 wt%, iron is 44.86 wt% and zirconia is 18.61 wt%. Carbon is formed during the removal of the binder from the specimen surface. On the basis of the above discussion it can be concluded that EDS of 5000X image shows more amount of iron as compared to the EDS of 25000X. Concentration of alumina, zirconia and oxygen was high in 25000X image.

8.1.3 Density

Fig. 8.15 shows the Density vs. Sintering Temperature plot of various 2.5Zr2.5AFe specimens for different time intervals. The Specimen 2.5Zr2.5AFe900(1) shows the density values of 4.881 gm/cm^3, the specimen 2.5Zr2.5AFe1000(1) showed the density value of 4.902 gm/cm^3 and the specimen 2.5Zr2.5AFe1100(1) showed the density value of 5.159 gm/cm^3 respectively. On increasing the sintering time to 2 hour, keeping the sintering temperature as 900, 1000 and 1100°C the three specimens were formed namely 2.5Zr2.5AFe900(2), 2.5Zr2.5AFe1000(2) and 2.5Zr2.5AFe1100(2). The specimen 2.5Zr2.5AFe900(2) showed the density value of 4.964 gm/cm^3, in the similar manner specimen 2.5Zr2.5AFe1000(2) showed the density value of 4.985 gm/cm^3 and specimen 2.5Zr2.5AFe1100(2) showed the density

value of 5.047 gm/cm^3. In its continuation specimen sintered for 3 hour at 900, 1000 and 1100°C i.e. 2.5Zr2.5AFe900(3), 2.5Zr2.5AFe1000(3) and 2.5Zr2.5AFe1100(3) showed density values of 5.003 gm/cm^3, 5.077 gm/cm^{3}and 5.039 gm/cm^3 respectively. It can be concluded from the above graphs that as we increase the sintering temperature the density value increases. It can be seen from the graph that for the specimens sintered at 1100°C the highest density value was observed for the specimen 2.5Zr2.5AFe1100(1). This may be due to the reason that at 1100°C sintering temperature and 1 hour of sintering time an optimum amount of the iron aluminate and iron zirconium oxide phase formation takes place.

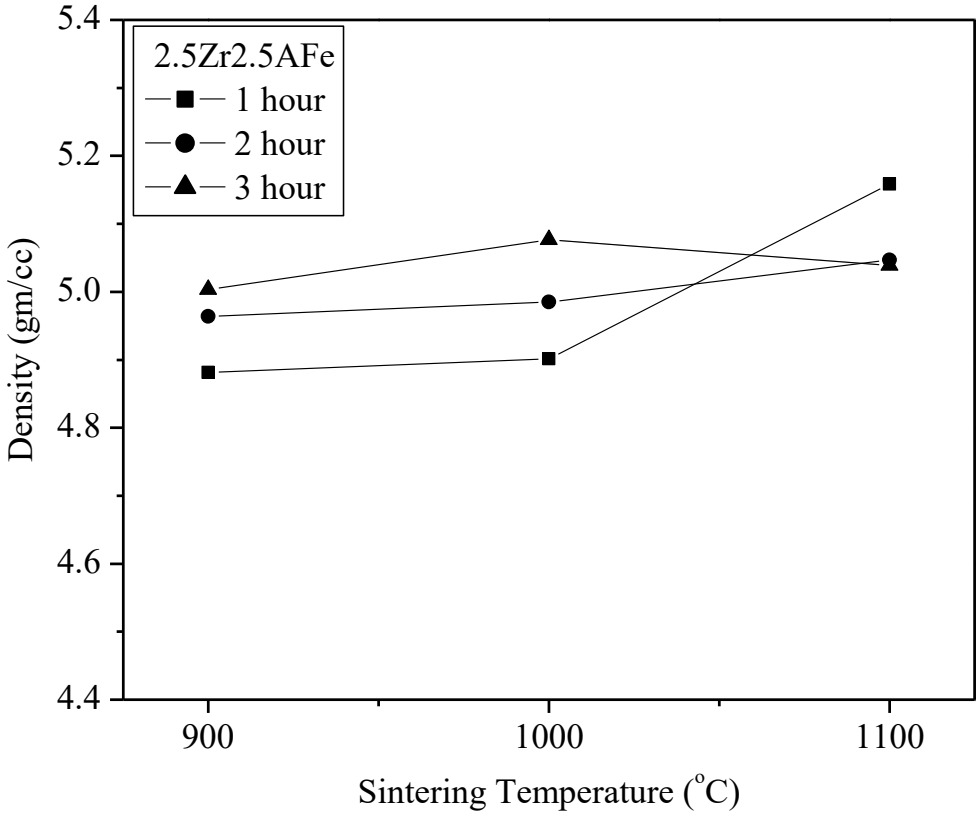

Fig. 8.15 Density vs. Sintering Temperature plot of various 2.5Zr2.5AFe specimens

8.1.4 Hardness

Fig. 8.16 shows the plot of hardness vs. sintering temperature of various 2.5Zr2.5AFe specimens for different sintering times. Specimen 2.5Zr2.5AFe900(1) shows a hardness number of 29 HRH whereas specimen 2.5Zr2.5AFe1000(1) shows hardness number of 44 HRH and finally specimen 2.5Zr2.5AFe1100(1) shows hardness number of 55 HRH. For the specimens sintered at 2 hour i.e. the specimen 2.5Zr2.5AFe900(2) showed hardness number of 30 HRH, specimen 2.5Zr2.5AFe1000(2) showed hardness number of 48 HRH whereas specimen 2.5Zr2.5AFe1100(2) showed hardness number of 56 HRH. Finally the last spate of the specimen revealed the hardness number of the specimen 2.5Zr2.5AFe900(3) as 31 HRH, for the specimen 2.5Zr2.5AFe1000(3) as 49 HRH and for the specimen 2.5Zr2.5AFe1100(3) as 59 HRH. It can be concluded from the above discussion that the hardness number of the various specimen increases with the increase in the sintering temperature as well as the sintering time respectively.

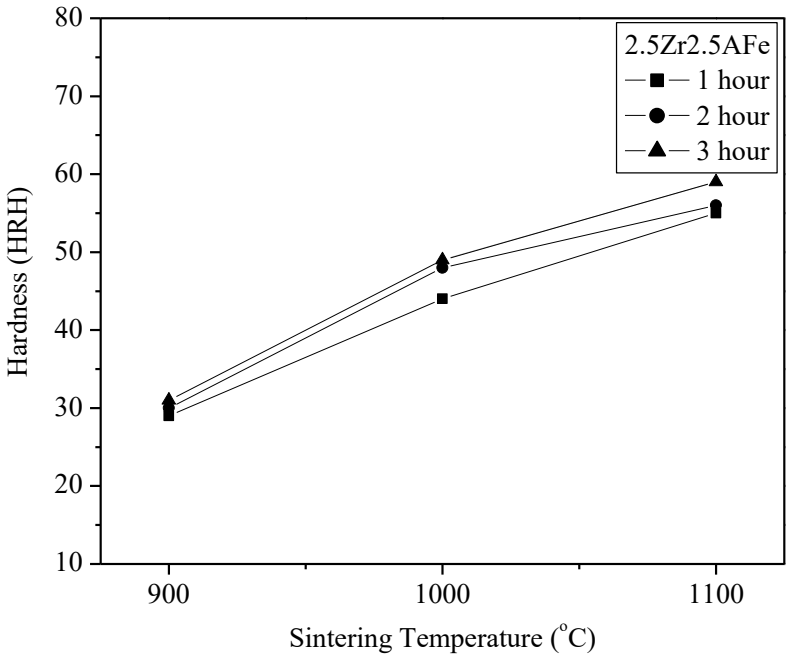

Fig. 8.16 Hardness vs. Sintering Temperature plot of various 2.5Zr2.5AFe specimens

8.1.5 Wear

Specimens sintered at 900°C for 1,2 and 3 hour time were found to have low strength due to incomplete sintering and are not able to sustain frictional load during wear test. Therefore, the wear behavior of 900°C sintered specimens was not recorded. Fig. 8.17 and table 8.3 shows the wear rate vs. load and values of wear rate at different loads respectively for specimen sintered at 1000°C for different sintering time intervals of 1, 2 and 3 hour respectively. At 1000°C the specimen sintered for 1 hour i.e. 2.5Zr2.5AFe1000(1) showed wear rate of 0.3448 mm^3/Km at a load of 0.5 kg, on increasing the load to 1.0 kg the same specimen showed a wear rate of 0.3739 mm^3/Km.

Table 8.3 Wear rate values of different 2.5Zr2.5AFe specimens at different loads

S. No.	Specimen Code	Wear Rate (mm^3/Km) at 0.5 Kg Load	Wear Rate (mm^3/Km) at 1.0 Kg Load	Wear Rate (mm^3/Km) at 1.5 Kg Load	Wear Rate (mm^3/Km) at 2.0 Kg Load
1.	2.5Zr2.5AFe1000(1)	0.3448	0.3739	0.4166	0.4884
2.	2.5Zr2.5AFe1000(2)	0.2384	0.2454	0.2555	0.3854
3.	2.5Zr2.5AFe1000(3)	0.2002	0.2122	0.2234	0.2442
4.	2.5Zr2.5AFe1100(1)	0.2452	0.2528	0.2612	0.3924
5.	2.5Zr2.5AFe1100(2)	0.1644	0.1843	0.2155	0.2736
6.	2.5Zr2.5AFe1100(3)	0.1582	0.1637	0.1957	0.2010

Further increase in the load to 1.5 kg load on the test rig showed wear rate value of 0.4166 mm^3/Km, at 2.0 kg load the same specimen showed the wear rate value of 0.4884 mm^3/Km. In the similar manner the specimen which was sintered for 2 hour i.e. 2.5Zr2.5AFe1000(2) showed wear rate value of 0.2384 mm^3/Km at a load of 0.5 kg, the same specimen when weared at a load of 1.0 kg showed the wear rate of

0.2454 mm^3/Km. Upon further increasing the load on the test rig to 1.5 kg, the same specimen showed wear rate value of 0.2555 mm^3/Km and when the same specimen was run at a load of 2.0 kg, it showed wear rate of 0.3854 mm^3/Km. The last specimen which was sintered at 1000°C for 3 hour i.e. the specimen 2.5Zr2.5AFe1000(3) showed the wear rate of 0.2002 mm^3/Km at load of 0.5 kg, the same specimen when run at 1.0 kg load shows a wear rate of 0.2122 mm^3/Km. The specimen showed wear rate of 0.2234 mm^3/Km at a load of 1.5 Kg and finally a wear rate of 0.2442 mm^3/Km was found at a load of 2.0 Kg respectively.

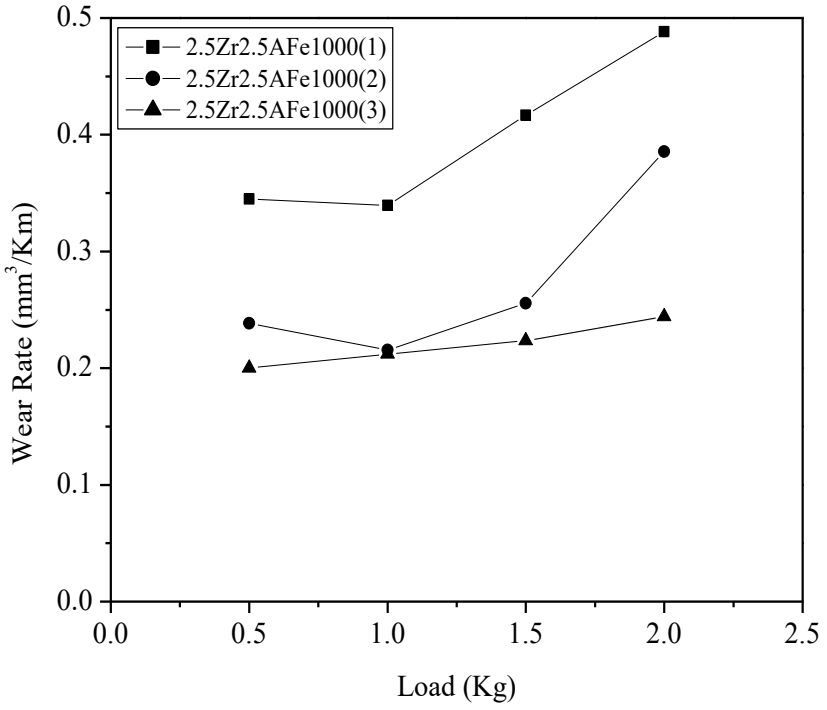

Fig. 8.17 Wear Rate vs. Load plot for specimen sintered at 1000°C

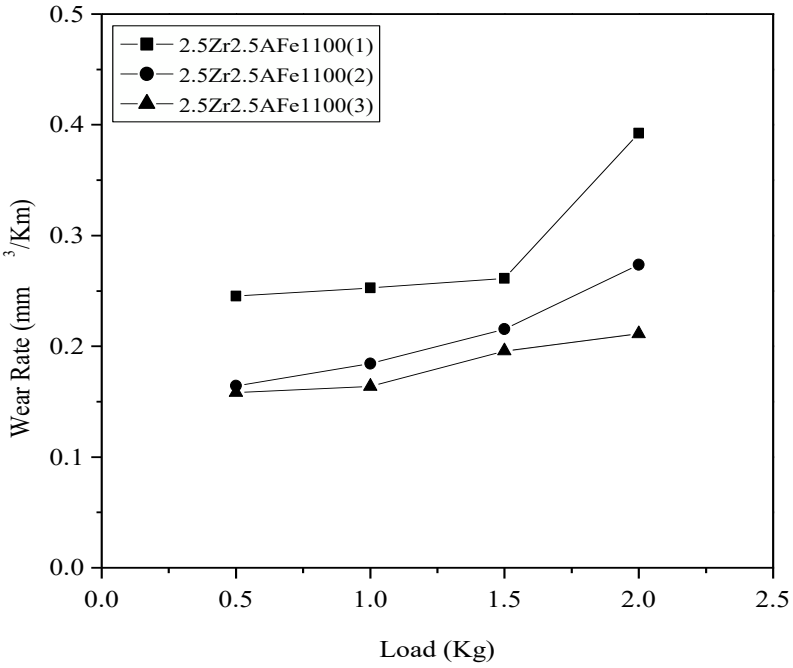

Fig. 8.18 Wear Rate vs. Load plot for specimen sintered at 1100°C

Fig. 8.18 and table 8.3 shows the wear rate vs. load and value of wear rate at different loads respectively for specimen sintered at 1100°C for different sintering time of 1, 2 and 3 hour respectively. The specimen 2.5Zr2.5AFe1100(1) showed wear rate of 0.2452 mm^3/Km at a load of 0.5 kg, at 1.0 kg load the same specimen showed wear rate of 0.2528 mm^3/Km, the same specimen when weared at a load of 1.5 kg showed wear rate of 0.2612 mm^3/Km and finally when the same specimen is weared at a load of 2.0 kg showed wear rate of 0.3924 mm^3/Km. In the similar manner the specimen 2.5Zr2.5AFe1100(2) showed wear rate of 0.1644 mm^3/Km at a load of 0.5 kg, on increasing the load to 1.0 kg the same specimen showed wear rate of 0.1843 mm^3/Km. Further increase in the values of load on the test rig from 1.5 kg to 2.0 kg showed the wear rate of 0.2155 mm^3/Km and 0.2736 mm^3/Km.

8.1.6 Scanning Electron Microscopy (After Wear)

Fig. 8.19 shows the worn SEM micrograph of the specimen 2.5Zr2.5AFe1000(1) at (a) 500X (b) 2000X (c) 5000X and (d) 25000X respectively. Fig. 8.19(a) shows

micrograph of the specimen at 500X showing the removal of material from the nanocomposite specimen due to entrapment of hard iron aluminate ($FeAl_2O_4$) and iron zirconium oxide (Zr_6Fe_3O) particles.

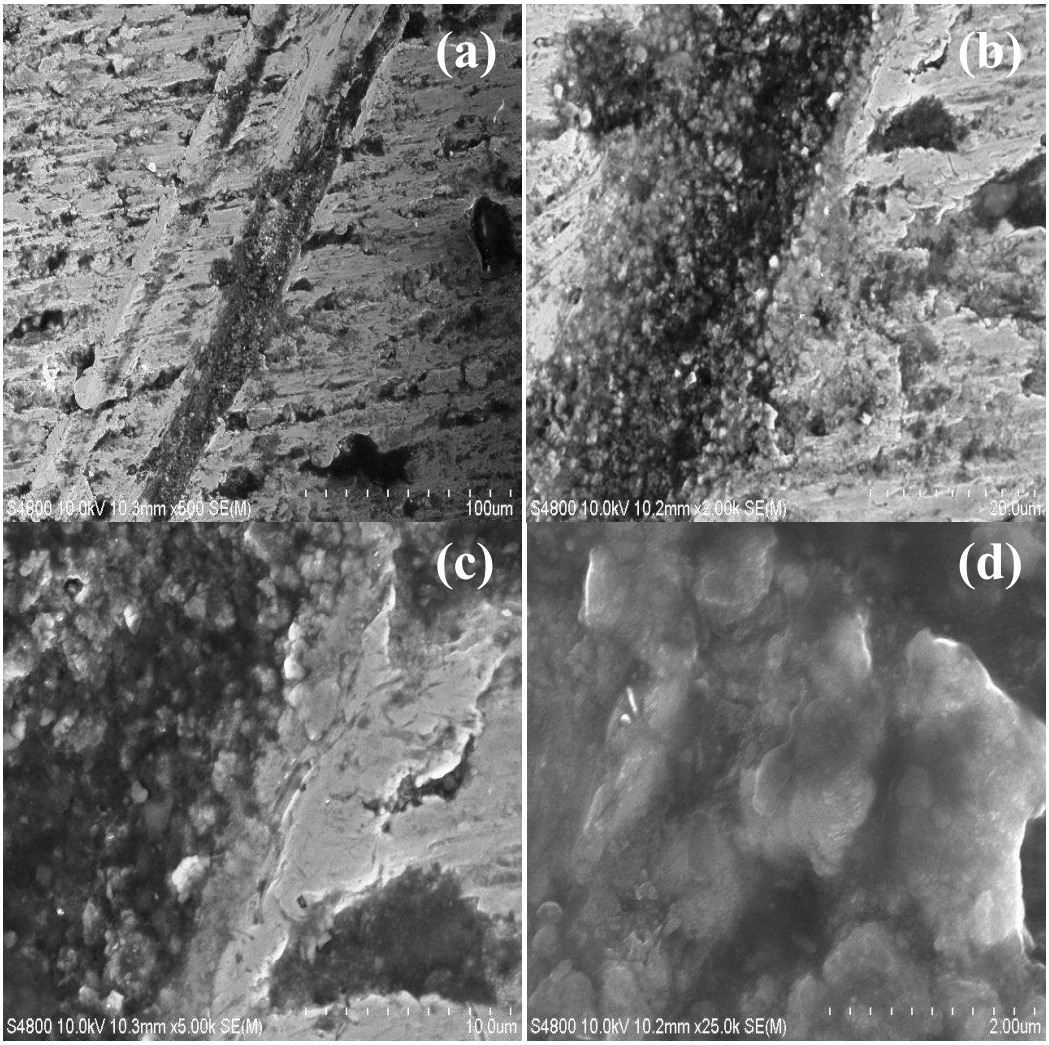

Fig. 8.19 Worn SEM micrograph of specimen 2.5Zr2.5AFe1000(1) at (a) 500X (b) 2000X (c) 5000X and (d) 25000X respectively

Fig. 8.19(b) shows the micrograph of the same specimen at 2000X magnification revealing the scoring mark generation during the tribofilm formation between the disc and the pin surface. Fig. 8.19(c) shows the micrograph of the same specimen at 5000X magnification which shows the nano size particles of iron aluminate and iron zirconium oxide particles respectively. Fig. 8.19(d) shows the micrograph of the specimen at 25000X illustrating the localized welding phenomenon between the

constituent reactive phases respectively. The overall mechanism in the present case was found to be abrasive in nature as there is peeling off the material in the intricate zones of the material which are having metallic characteristics. Due to these metallic characteristics there is a groove generation on the specimen surface.

Fig. 8.20 shows the worn SEM micrograph of the specimen 2.5Zr2.5AFe1100(1) at (a) 500X (b) 2000X (c) 5000X and (d) 25000X respectively. Fig. 8.20(a) shows micrograph of the specimen at 500X showing the removal of material from the nanocomposite specimen due to the presence of nano reactive phases respectively.

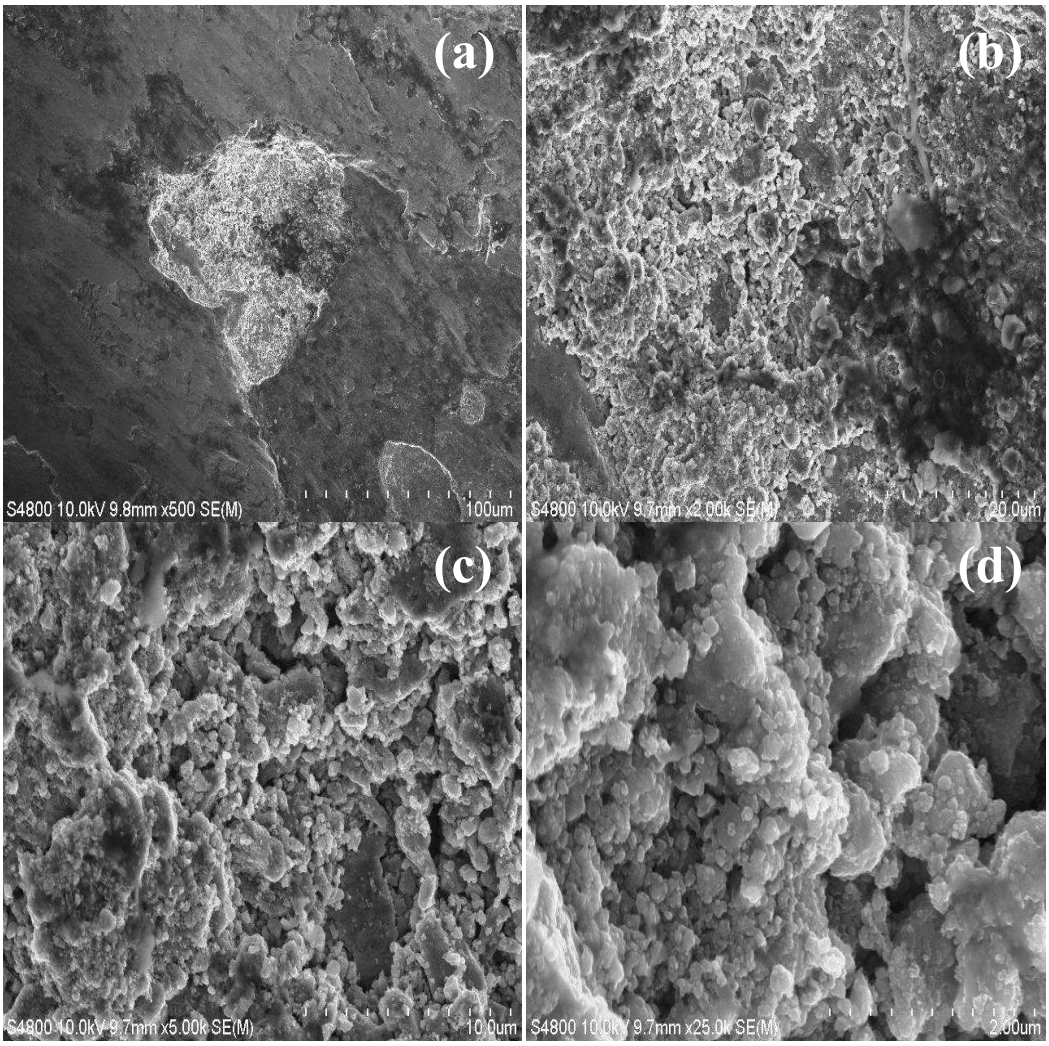

Fig. 8.20 Worn SEM micrograph of specimen 2.5Zr2.5AFe1100(1) at (a) 500X (b) 2000X (c) 5000X and (d) 25000X respectively

Fig. 8.20(b) shows the micrograph of the same specimen at 2000X magnification revealing the area from where the material has been removed during the dry sliding wear test. Fig. 8.20(c) shows the micrograph of the same specimen at 5000X magnification which shows the nano size particles of iron aluminate and iron zirconium oxide particles respectively. Fig. 8.20(d) shows the micrograph of the specimen at 25000X illustrating the strong bonding between the constituent reactive phases. In the present case, it can be seen that the removal of the material is due to the adhesive wear. Due to this adhesive wear, the scoring mark are not intense due to which there is a polishing effect on the specimen surface.

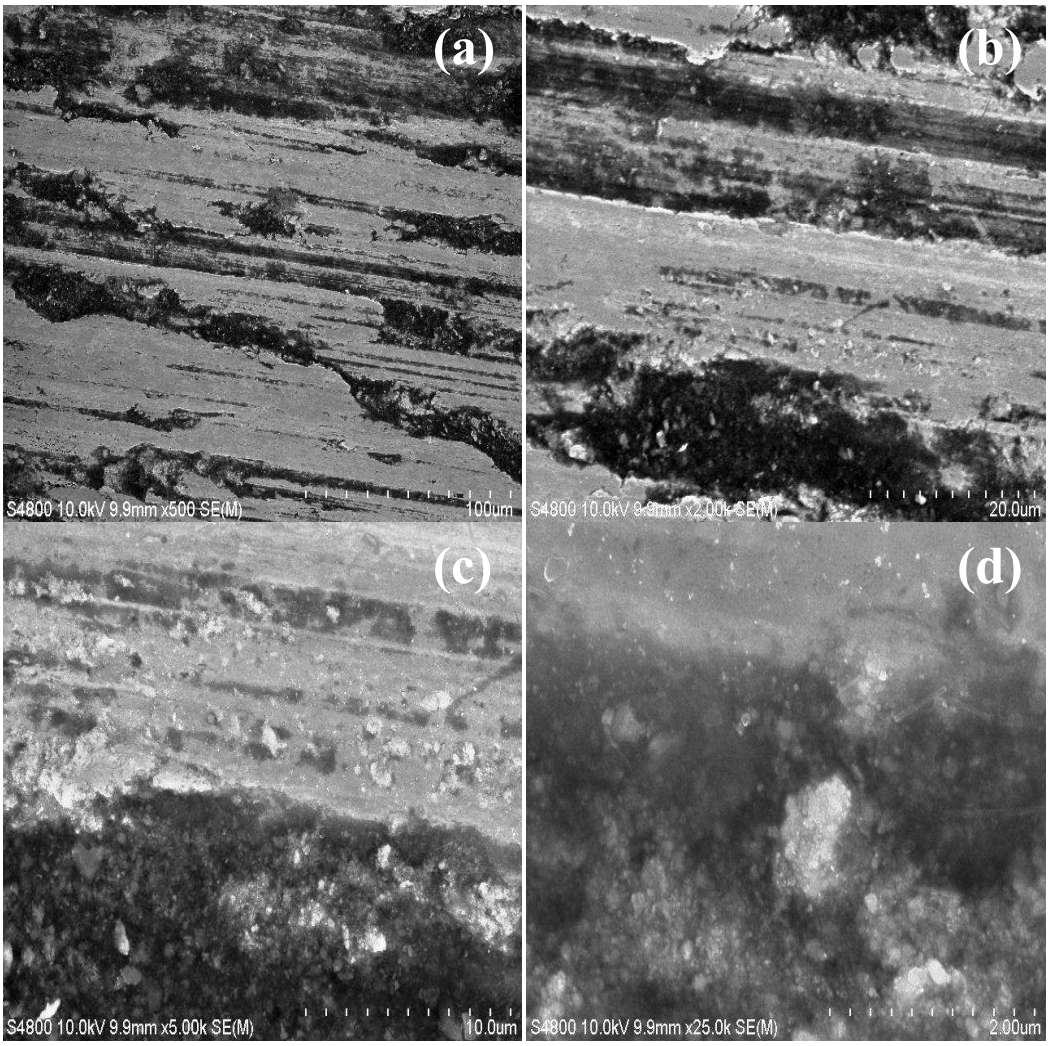

Fig. 8.21 Worn SEM micrograph of specimen 2.5Zr2.5AFe1100(2) at (a) 500X (b) 2000X (c) 5000X and (d) 25000X respectively

Fig. 8.21 shows the worn SEM micrograph of specimen 2.5Zr2.5AFe1100(2) at (a) 500X (b) 2000X (c) 5000X and (d) 25000X respectively. Fig. 8.21(a) shows micrograph of the specimen at 500X showing the removal of material as well as polishing on the nanocomposite specimen. The removal of the material in the present case may be attributed due to the entrapment of the hard debris between the disc and pin. Fig. 8.21(b) shows the micrograph of the same specimen at 2000X magnification revealing the crack generation in the grooves of the specimen surface. Fig. 8.21(c) shows the micrograph of the same specimen at 5000X magnification which shows the nano size particles of iron aluminate and iron zirconium oxide respectively. Fig. 8.21(d) shows the micrograph of the specimen at 25000X illustrating the strong bonding between the constituent reactive phases respectively.

8.2) Structural and Mechanical Characterization of 3.5Zr1.5AFe Hybrid Metal Matrix Nanocomposites System

8.2.1 X-Ray Diffraction

Fig. 8.22 shows the XRD plots of the specimen (a) 3.5Zr1.5AFe900(1) (b) 3.5Zr1.5AFe900(2) and (c) 3.5Zr1.5AFe900(3). All the identified peaks were matched with the JCPDS data file. Specimen 3.5Zr1.5AFe900(1) shows the peaks of iron and iron aluminate phase. Specimen 3.5Zr1.5AFe900(2) shows the presence of iron, aluminium oxide and iron zirconium oxide phases respectively. Further, specimen 3.5Zr1.5AFe900(3) shows the presence of iron, alumina, iron aluminate and iron zirconium oxide phases respectively. Iron aluminate and iron zirconium oxide phases are formed due to the reactive sintering between the iron – alumina and iron – zirconia particles respectively.

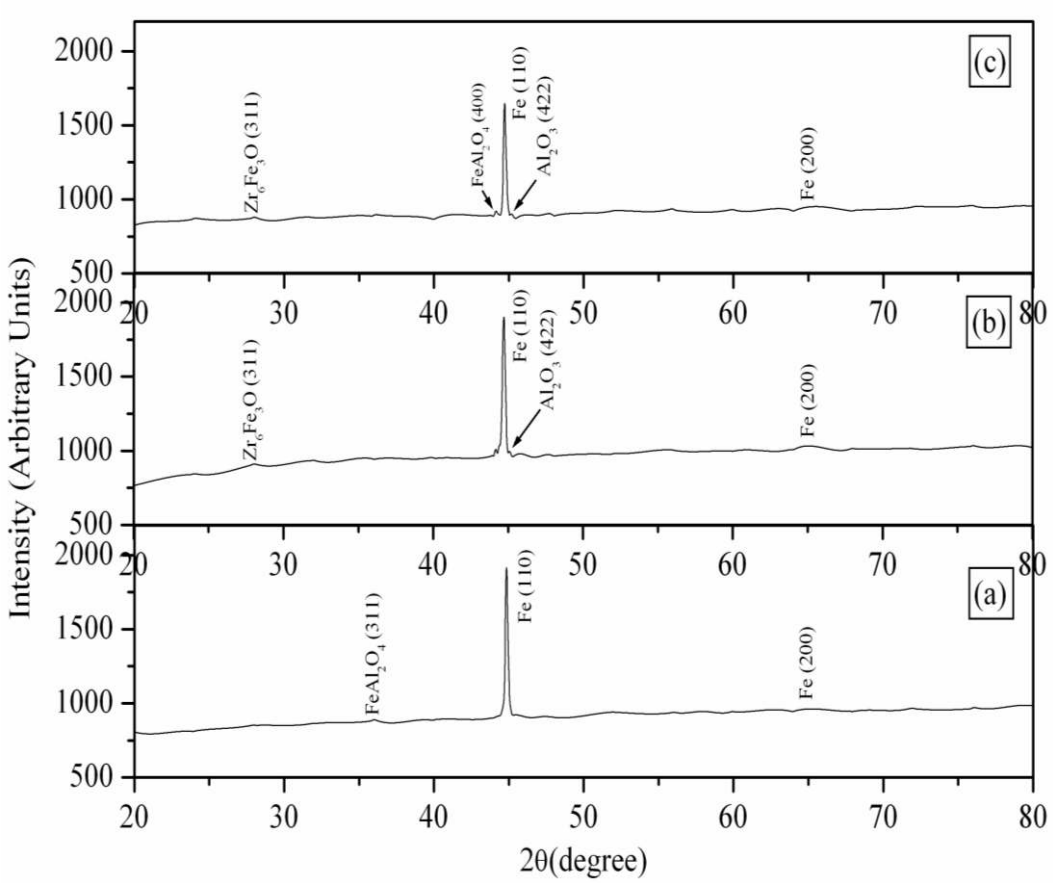

Fig. 8.22 XRD plots of specimen (a) 3.5Zr1.5AFe900(1) (b) 3.5Zr1.5AFe900(2) and (c) 3.5Zr1.5AFe900(3)

Fig. 8.23 shows the XRD plots of the specimen 3.5Zr1.5AFe1000(1), 3.5Zr1.5AFe1000(2) and 3.5Zr1.5AFe1000(3) respectively. All the identified peaks were matched with the JCPDS data file. Specimen 3.5Zr1.5AFe1000(1) shows the presence of peaks of iron (Fe), aluminium oxide (Al_2O_3) and zirconium dioxide (ZrO_2) along with the presence of some traces of iron aluminate ($FeAl_2O_4$) and iron zirconium oxide (Zr_6Fe_3O) phase respectively. In the similar manner, specimen 3.5Zr1.5AFe1000(2) also showed the presence of Fe, Al_2O_3 and ZrO_2 along with some trace amount of $FeAl_2O_4$ and Zr_6Fe_3O phase. Again the specimen which was sintered at 1000°C for 3 hour i.e. 3.5Zr1.5AFe1000(3) shows the presence of Fe, Al_2O_3 and ZrO_2 along with some trace amount of iron zirconium oxide (Zr_6Fe_3O) and iron aluminate ($FeAl_2O_4$) phase. It can be seen that the amount of iron aluminate and iron zirconium oxide phase was maximum in the specimen 3.5Zr1.5AFe1000(3).

Therefore it can be concluded on the basis of the above discussion that the amount of the reactive phases increases on increasing the sintering time.

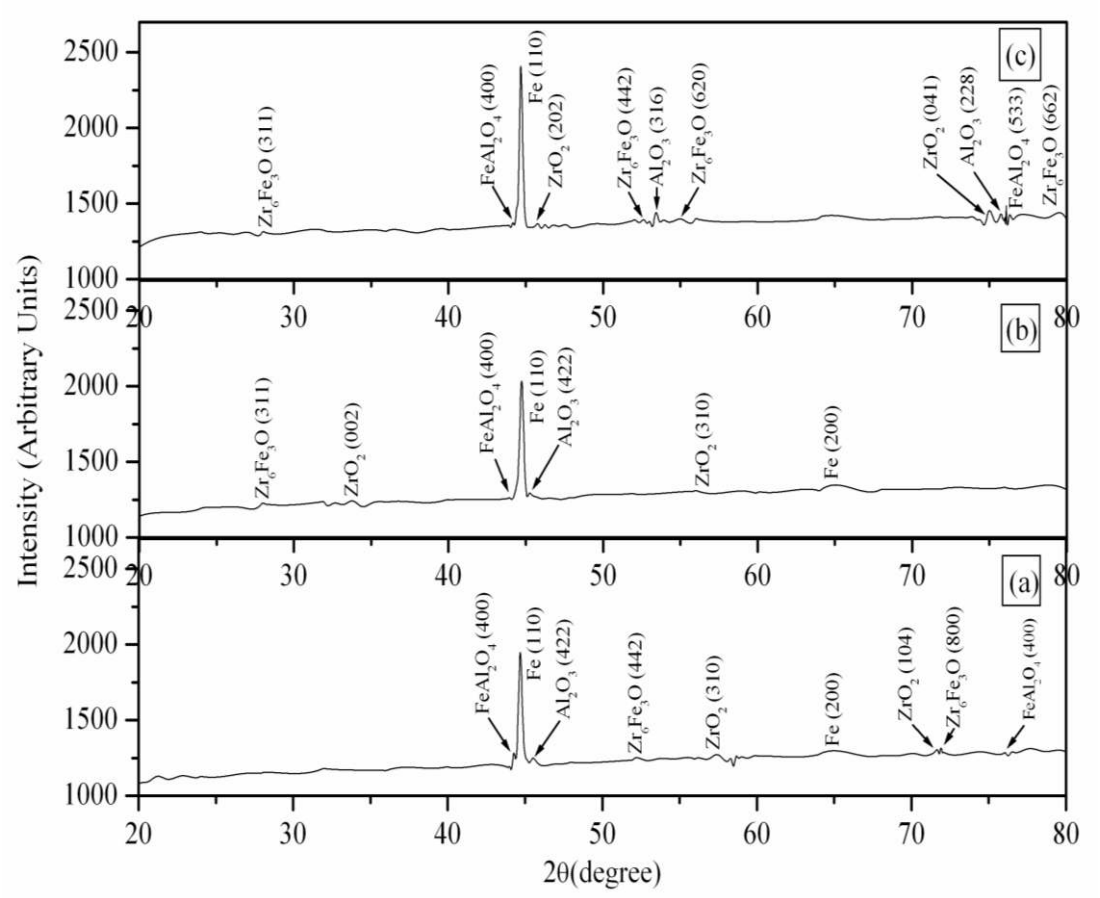

Fig. 8.23 XRD plots of specimen (a) 3.5Zr1.5AFe1000(1) (b) 3.5Zr1.5AFe1000(2) and (c) 3.5Zr1.5AFe1000(3)

Fig. 8.24 shows XRD plots of the specimen 3.5Zr1.5AFe1100(1), 3.5Zr1.5AFe1100(2) and 3.5Zr1.5AFe1100(3). Specimen 3.5Zr1.5AFe1100(1) shows the presence of peaks of iron (Fe), aluminium oxide (Al_2O_3) and zirconium dioxide (ZrO_2) along with some traces of iron aluminate ($FeAl_2O_4$) and iron zirconium oxide (Zr_6Fe_3O) phase. In the similar manner, specimen 3.5Zr1.5AFe1100(2) shows the presence of peaks of iron (Fe), aluminium oxide (Al_2O_3) and zirconium dioxide (ZrO_2) along with the presence of some traces of iron aluminate ($FeAl_2O_4$) and iron zirconium oxide (Zr_6Fe_3O) phase. The specimen sintered for 3h i.e. specimen 3.5Zr1.5AFe1100(3) shows the presence of iron (Fe), aluminium oxide (Al_2O_3) and

zirconium dioxide (ZrO_2) along with some traces of iron aluminate ($FeAl_2O_4$) and iron zirconium oxide (Zr_6Fe_3O) phase respectively. It can be concluded on the basis of the above discussion that the highest amount of the iron aluminate as well as the iron zirconium oxide phases were present in the specimen 3.5Zr1.5AFe1100(1).

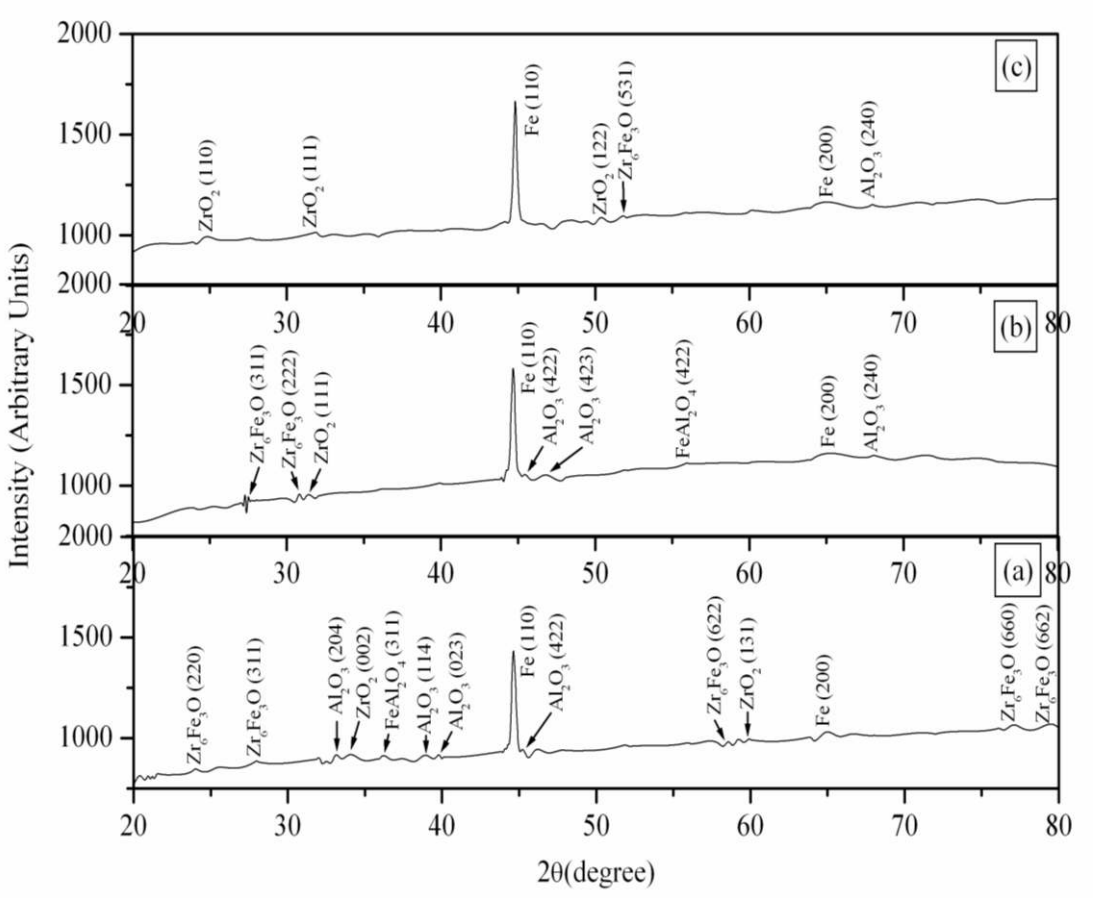

Fig. 8.24 XRD plots of specimen (a) 3.5Zr1.5AFe1100(1) (b) 3.5Zr1.5AFe1100(2) and (c) 3.5Zr1.5AFe1100(3)

8.2.2 Scanning Electron Microscopy (As Prepared)

Fig. 8.25 shows the SEM micrograph of specimen 3.5Zr1.5AFe900(1) at (a) 500X (b) 1000X (c) 5000X and (d) 20000X respectively. Fig. 8.25(a) shows the electron microscopic image of the specimen at 500X illustrating the conjugate grains of the composite structure. Specimen also shows the presence of some minute amount of pores. Presence of connected pores can be seen in the present case. The same specimen when viewed at 1000X [Fig. 8.25(b)] shows the presence of bigger size

grains of iron distributed uniformly over the entire area. Fig. 8.25(c) shows the SEM image of the specimen at 5000X illustrating the presence of some fine grains of iron aluminate phase. Iron aluminate phase forms as a result of reactive sintering between iron and alumina particles. Fig. 8.25(d) describes the electron microscopic image of the same specimen at 20000X which shows the nano size grains of the iron aluminate phase. The nano size grains of iron aluminate phase are found to be present on the surface of large size grains of iron. Apart from the nano size grains of iron aluminate phase are found to be present on the grain as well as on the grain boundary.

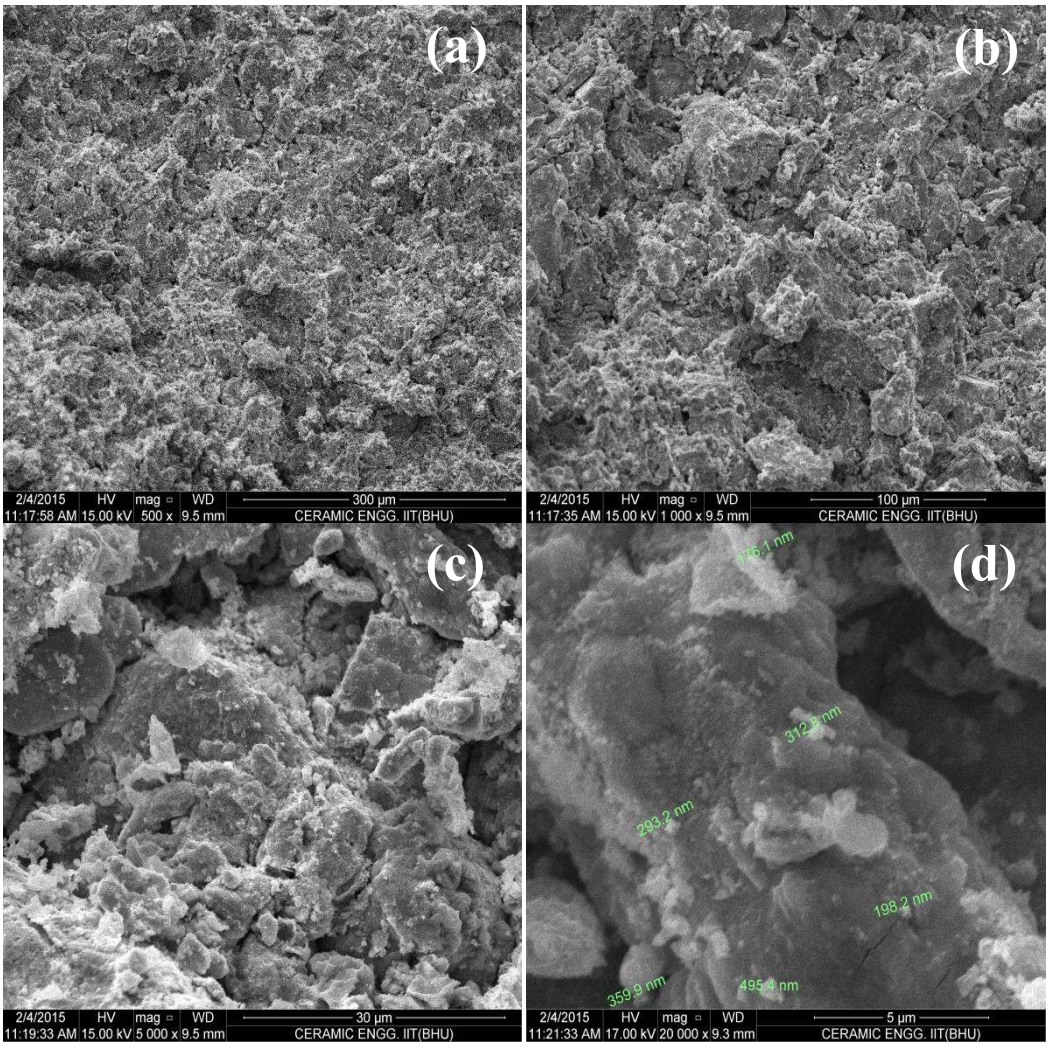

Fig. 8.25 SEM micrograph of specimen 3.5Zr1.5AFe900(1) at (a) 500X (b) 1000X (c) 5000X and (d) 20000X respectively

Fig. 8.26 shows the SEM micrograph of specimen 3.5Zr1.5AFe900(2) at (a) 500X (b) 1000X (c) 5000X and (d) 20000X respectively. Fig. 8.26(a) shows the SEM image of the specimen at 500X illustrating uniformly distributed loosely bound grains of the composite structure. Fig. 8.26(b) shows the electron microscopic image of the same specimen at 1000X revealing the grains of iron along with some grains of aluminium oxide.

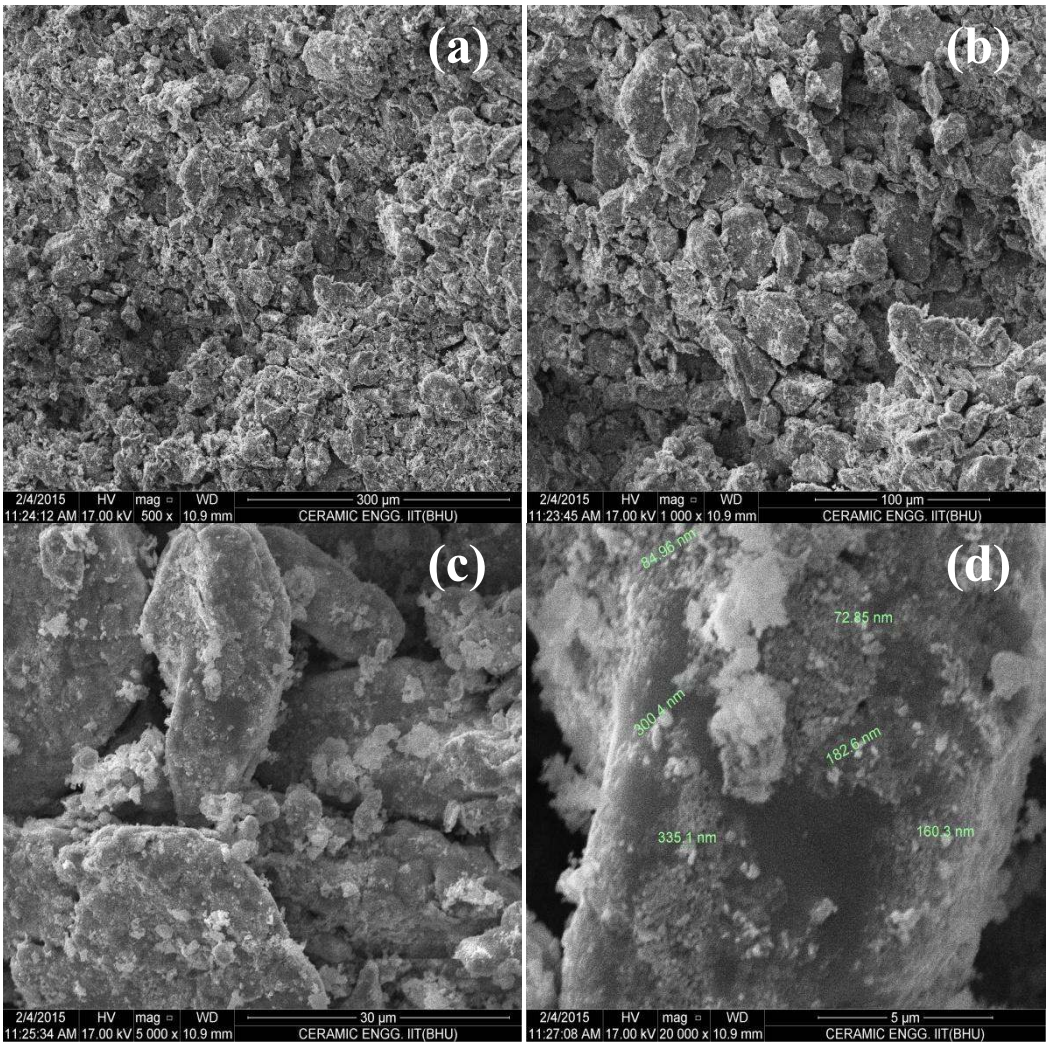

Fig. 8.26 SEM micrograph of specimen 3.5Zr1.5AFe900(2) at (a) 500X (b) 1000X (c) 5000X and (d) 20000X respectively

The same specimen when viewed at 5000X [Fig. 8.26(c)] shows the micron and sub micron size grains of iron aluminate and iron zirconium oxide phase respectively. Fig.

8.26(d) illustrates the electron microscopic image of the same specimen at 20000X showing the nano size grains of iron aluminate and iron zirconium oxide phases respectively. Nano size grains are found to be sticked on the surface of the grain of iron respectively.

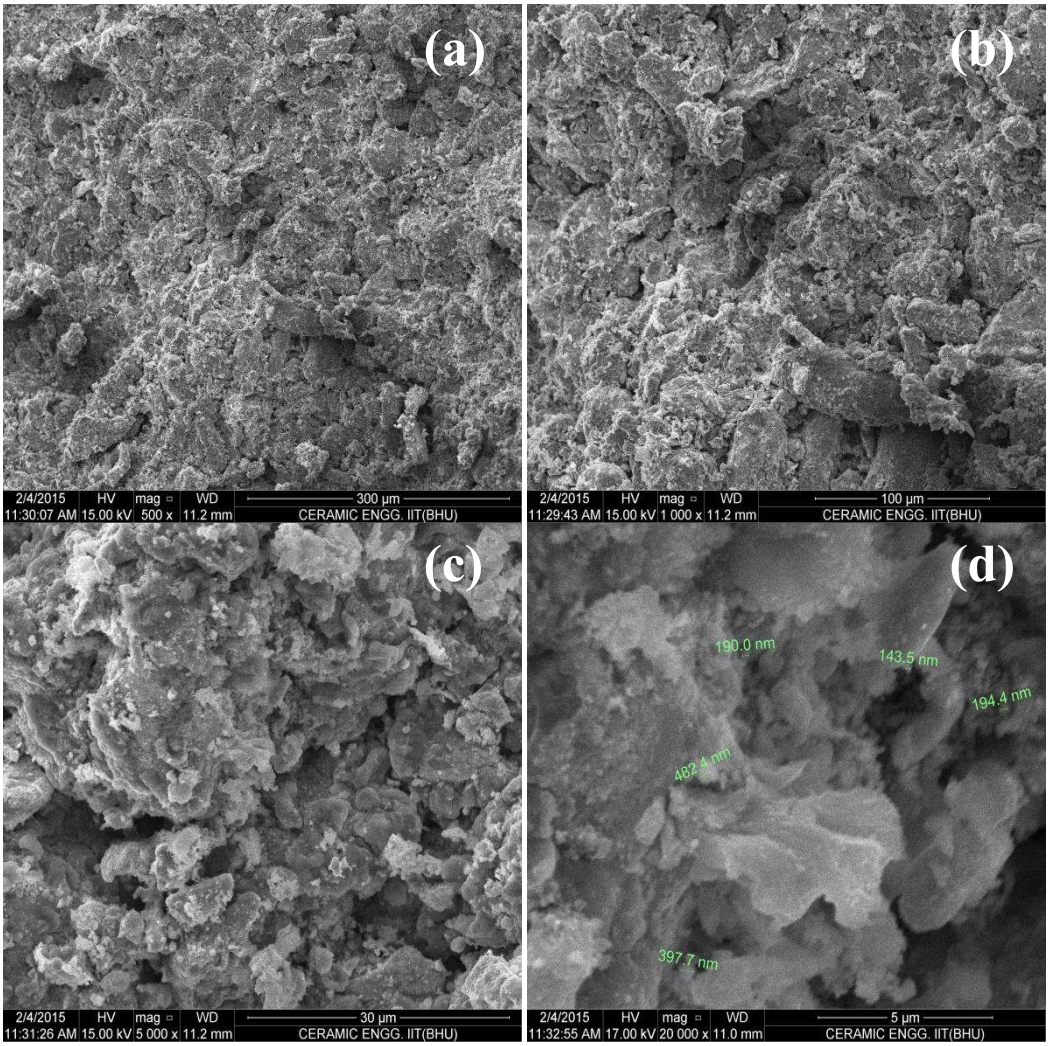

Fig. 8.27 SEM micrograph of specimen 3.5Zr1.5AFe900(3) at (a) 500X (b) 1000X (c) 5000X and (d) 20000X respectively

Fig. 8.27 shows the SEM micrograph of specimen 3.5Zr1.5AFe900(3) at (a) 500X (b) 1000X (c) 5000X and (d) 20000X respectively. Fig. 8.27(a) shows the SEM micrograph of the specimen at 500X revealing finer size loose grains of the composite structure. However, due to low temperature but higher time of sintering leads to small amount of densification still the present specimen is little bit denser in comparison to the specimen 3.5Zr1.5AFe900(1) and 3.5Zr1.5AFe900(2). Same

specimen when viewed at 1000X [Fig. 8.27(b)] shows the accumulated large size grains of iron along with the some sub micron size grains of alumina sticked on the periphery of iron grains. Fig. 8.27(c) shows the electron micrograph of the same specimen at 5000X revealing 4-6 μm size grains of iron. Some small grains of iron of size 0.5-1.0 μm are also present. Fig. 8.27(d) shows the scanning electron micrograph of the specimen at 20000X which shows the nano size grains of iron aluminate and iron zirconium oxide formed due to reactive sintering between iron-alumina and iron-zirconia particles. The size of the iron zirconium oxide particles are found to be small in comparison to the specimen 3.5Zr1.5AFe900(1) and 3.5Zr1.5AFe900(2).

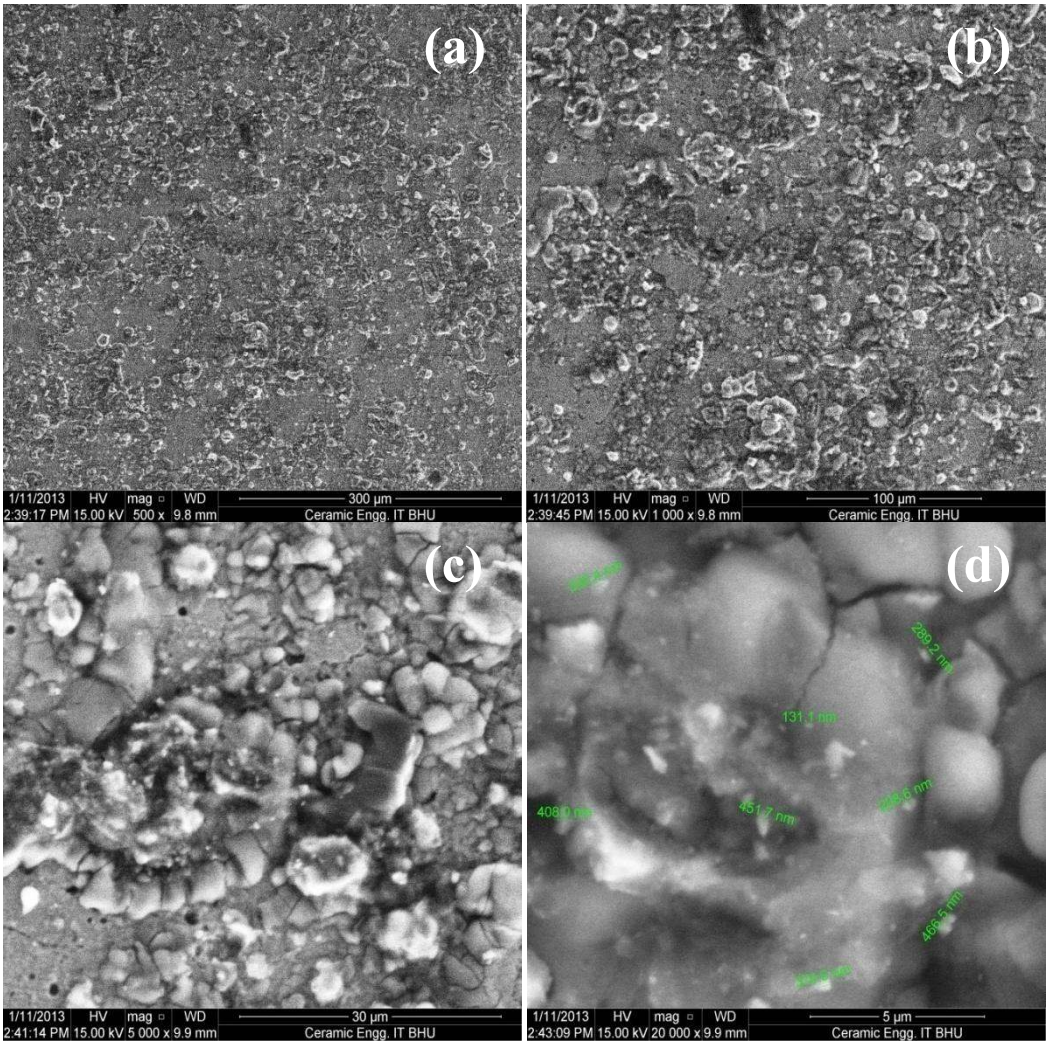

Fig. 8.28 SEM micrograph of specimen 3.5Zr1.5AFe1000(1) at (a) 500X (b) 1000X (c) 5000X and (d) 20000X respectively

Fig. 8.28 shows the SEM micrograph of the specimen 3.5Zr1.5AFe1000(1) at (a) 500X (b) 1000X (c) 5000X and (d) 20000X respectively. Fig. 8.28(a) shows the scanning electron microscopic image of the specimen at 500X revealing highly dense phase structure with the presence of negligible amount of porosity. Fig. 8.28(b) shows the SEM image of the specimen at 1000X illustrating the separate and distinct grains of the hybrid nanocomposite. Strong bonding between the various reactive phases can be very easily seen in the present micrograph. Fig. 8.28(c) shows the SEM image of the same specimen at 5000X which shows grains of Fe, Al_2O_3, ZrO_2 along with some sub micron size grains of iron aluminate $FeAl_2O_4$ and iron zirconium oxide (Zr_6Fe_3O) phases respectively. Fig. 8.28(d) shows the SEM image of the same specimen at 20000X revealing the presence of nano size particles of iron aluminate and iron zirconium oxide particles respectively. The size of the nano particles lies in the range of 130-450 nm respectively.

Fig. 8.29 shows the SEM micrograph of specimen 3.5Zr1.5AFe1100(1) at (a) 500X (b) 1000X (c) 5000X and (d) 20000X respectively. Fig. 8.29(a) shows the SEM image of the specimen at 500X revealing highly dense phase structure with negligible amount of porosity. Fig. 8.29(b) shows the electron microscopic image of the specimen at 1000X illustrating the conjugate and distinct grains of the hybrid nanocomposite. Strong bonding between the various reactive phases can also be very easily seen in the present micrograph. Fig. 8.29(c) shows the SEM image of the same specimen at 5000X which shows grains of Fe, Al_2O_3, ZrO_2 phases along with some sub micron size grains of iron aluminate $FeAl_2O_4$ and iron zirconium oxide (Zr_6Fe_3O) phases respectively. Fig. 8.29(d) shows the SEM image of the same specimen at 20000X revealing the presence of nano size particles of iron aluminate and iron zirconium oxide particles. The size of the nano particles lies in the range of 160-530 nm. It is also seen that nano size particles are found in the intergranular porosity.

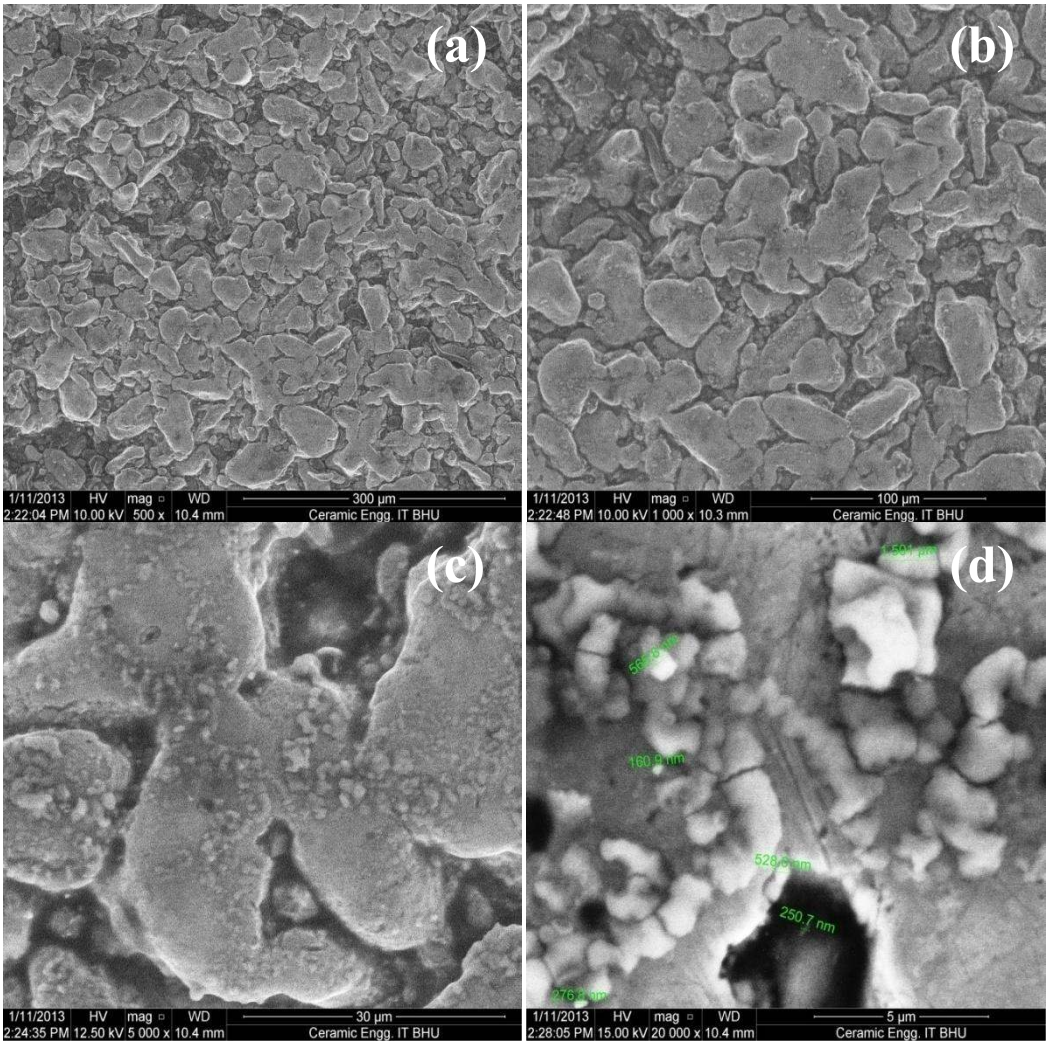

Fig. 8.29 SEM micrograph of specimen 3.5Zr1.5AFe1100(1) at (a) 500X (b) 1000X (c) 5000X and (d) 20000X respectively

Fig. 8.30 shows the SEM micrograph of the specimen 3.5Zr1.5AFe1100(2) at (a) 500X (b) 1000X (c) 5000X and (d) 20000X respectively. Fig. 8.30(a) shows the SEM image of the specimen at 500X revealing highly dense phase structure with the presence of negligible amount of porosity. Fig. 8.30(b) shows the electron microscopic image of the specimen at 1000X illustrating the conjugate and distinct grains of the hybrid nanocomposite. Strong bonding between the various reactive phases can also be very easily seen in the present micrograph. Fig. 8.30(c) shows the SEM image of the same specimen at 5000X which shows grains of Fe, Al_2O_3, ZrO_2 phases along with some sub micron size grains of iron aluminate $FeAl_2O_4$ and iron

zirconium oxide (Zr_6Fe_3O) phases. Fig. 8.30(d) shows the SEM image of the same specimen at 20000X revealing the presence of nano size particles of iron aluminate and iron zirconium oxide particles. The size of the nano particles lies in the range of 70-450 nm. It is also seen that nano size particles are found in the intergranular and intragranular porosity.

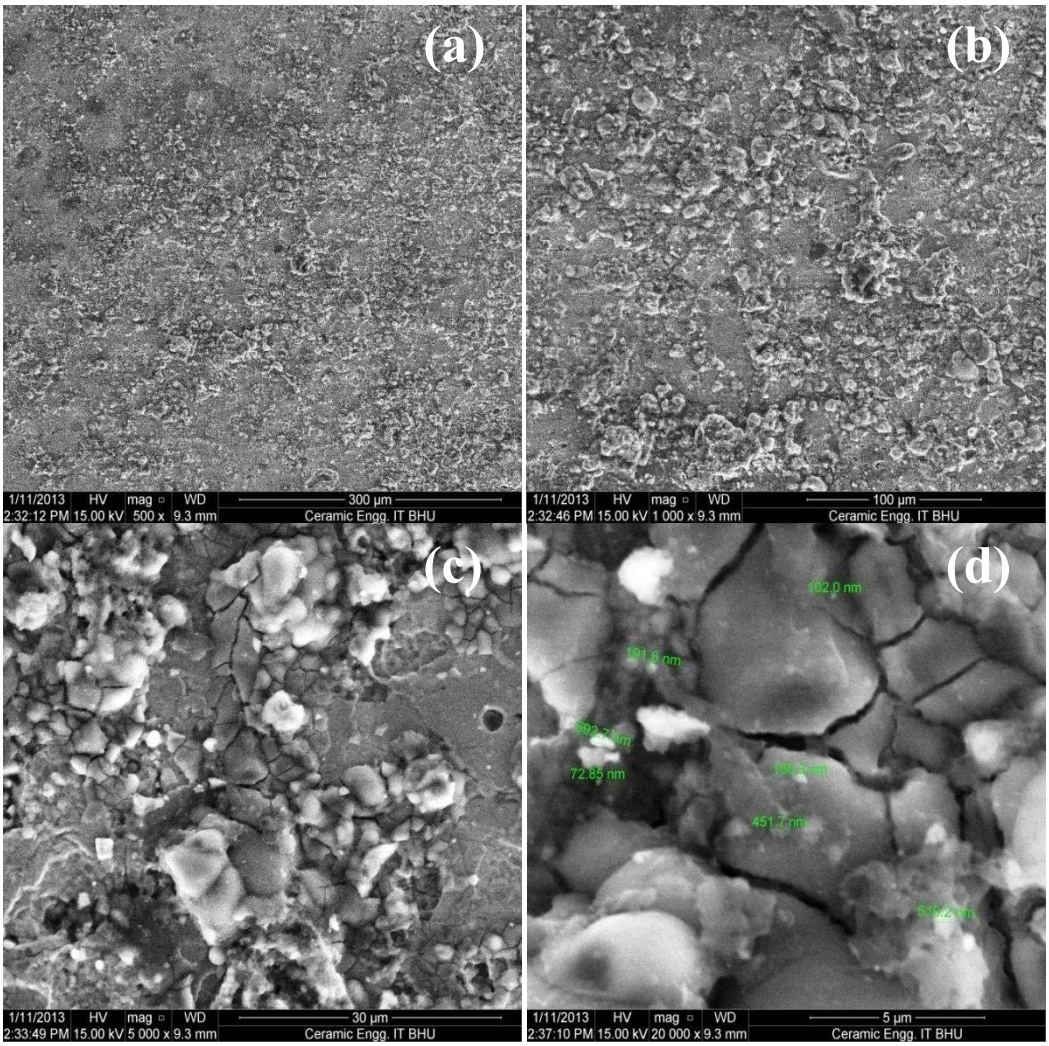

Fig. 8.30 SEM micrograph of specimen 3.5Zr1.5AFe1100(2) at (a) 500X (b) 1000X (c) 5000X and (d) 20000X respectively

Fig. 8.31 shows the SEM micrograph of specimen 3.5Zr1.5AFe1100(3) at (a) 500X (b) 1000X (c) 5000X and (d) 20000X respectively. Fig. 8.31(a) shows the SEM image of the specimen at 500X revealing highly dense phase structure with the presence of negligible amount of porosity. Fig. 8.31(b) shows the electron

microscopic image of the specimen at 1000X illustrating the conjugate and distinct grains of the hybrid nanocomposite. Strong bonding between the various reactive phases can also be very easily seen in the present micrograph.

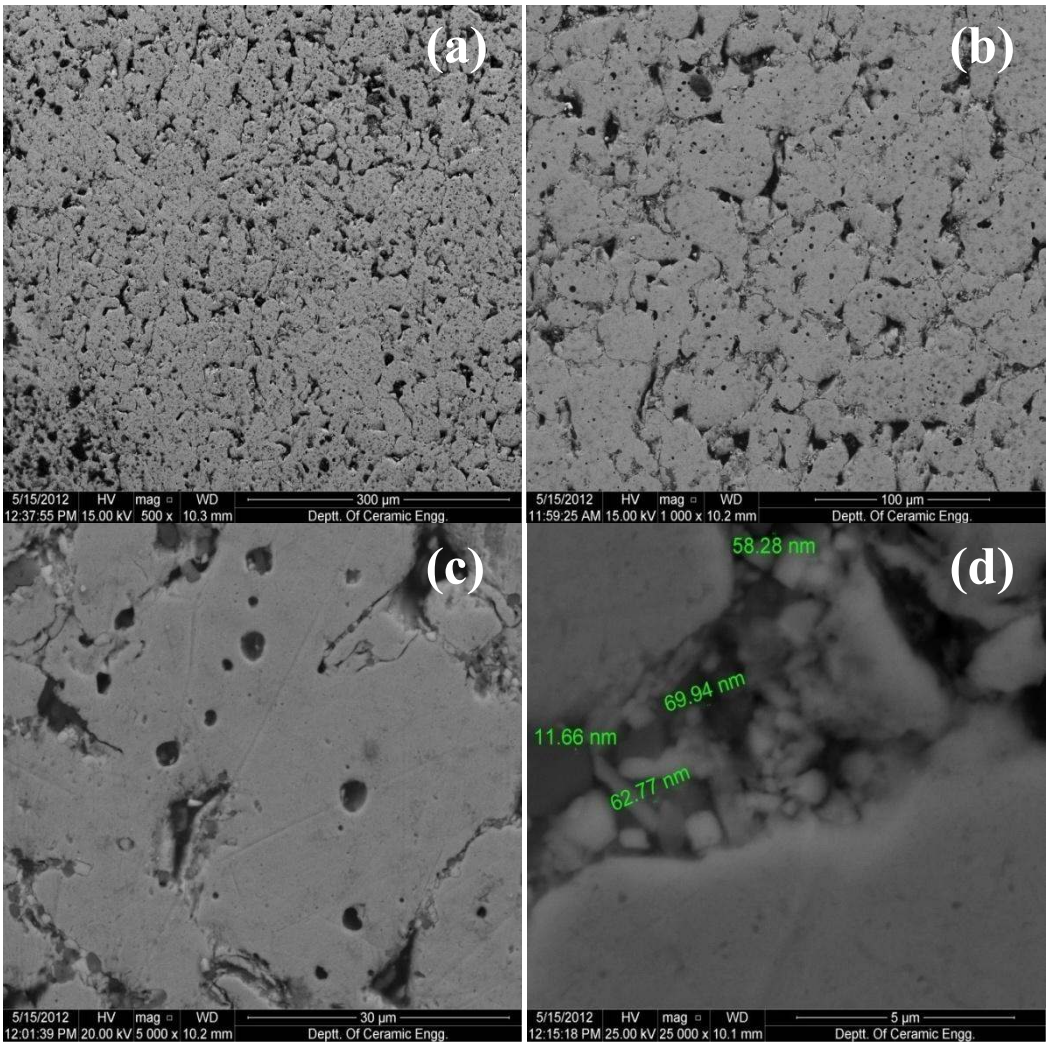

Fig. 8.31 SEM micrograph of specimen 3.5Zr1.5AFe1100(3) at (a) 500X (b) 1000X (c) 5000X and (d) 25000X respectively

Fig. 8.31(c) shows the SEM image of the same specimen at 5000X which shows grains of Fe, Al_2O_3, ZrO_2 phases along with some sub micron size grains of iron aluminate $FeAl_2O_4$ and iron zirconium oxide (Zr_6Fe_3O) phases. Fig. 8.31(d) shows the SEM image of the same specimen at 20000X revealing the presence of nano size particles of iron aluminate and iron zirconium oxide particles. The size of the nano

particles lies in the range of 70-450 nm respectively. It is also seen that nano size particles are found in the intergranular and intragranular porosity.

8.2.3 Density

Fig. 8.32 shows the density vs. sintering temperature plots of various 3.5Zr1.5AFe specimens. The green density of the specimen was found to lie between 4.804 gm/cc to 4.869 gm/cc. Specimen 3.5Zr1.5AFe900(1) showed sintered density value of 4.911 gm/cc, specimen 3.5Zr1.5AFe1000(1) showed sintered density value of 4.974 gm/cc and specimen 3.5Zr1.5AFe1100(1) showed sintered density value of 4.976 gm/cc.

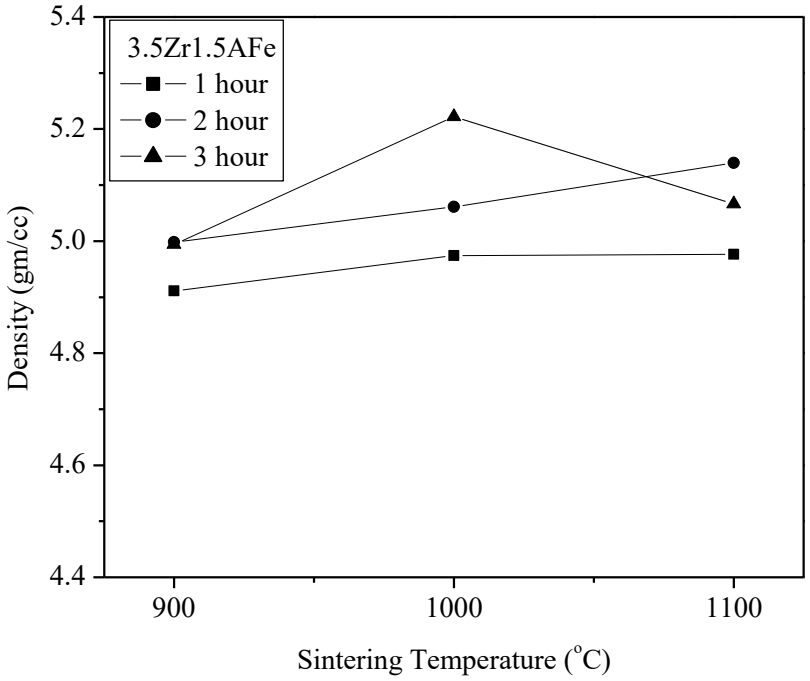

Fig. 8.32 Density vs. Sintering Temperature plot of various 3.5Zr1.5AFe specimens

On increasing the sintering time to 2 hours three specimens were formed namely 3.5Zr1.5AFe900(2), 3.5Zr1.5AFe1000(2) and 3.5Zr1.5AFe1100(2) respectively. These three specimens showed density of 4.998 gm/cc, 5.061 gm/cc and 5.140 gm/cc respectively. On increasing the sintering time to 3 hours, the specimen

3.5Zr1.5AFe900(3) showed sintered density value of 4.994 gm/cc, 3.5Zr1.5AFe1000(3) showed sintered density of 5.222 gm/cc and 3.5Zr1.5AFe1100(3) showed sintered density of 5.067 gm/cc respectively. It can be concluded on the basis of the above discussion that the sintered density increases as we increase the sintering temperature and time respectively.

8.2.4 Hardness

Fig. 8.33 shows hardness vs. sintering temperature plot of various 3.5Zr1.5AFe specimens. Hardness of the specimen 3.5Zr1.5AFe900(1) was found to be 32 HRH, specimen 3.5Zr1.5AFe1000(1) showed hardness number of 46 HRH and specimen 3.5Zr1.5AFe1100(1) showed hardness number of 53. On increasing the sintering time to 2 hour, the specimen 3.5Zr1.5AFe900(2), 3.5Zr1.5AFe1000(2) and 3.5Zr1.5AFe1100(2) showed hardness number of 33 HRH, 49 HRH and 56 HRH respectively.

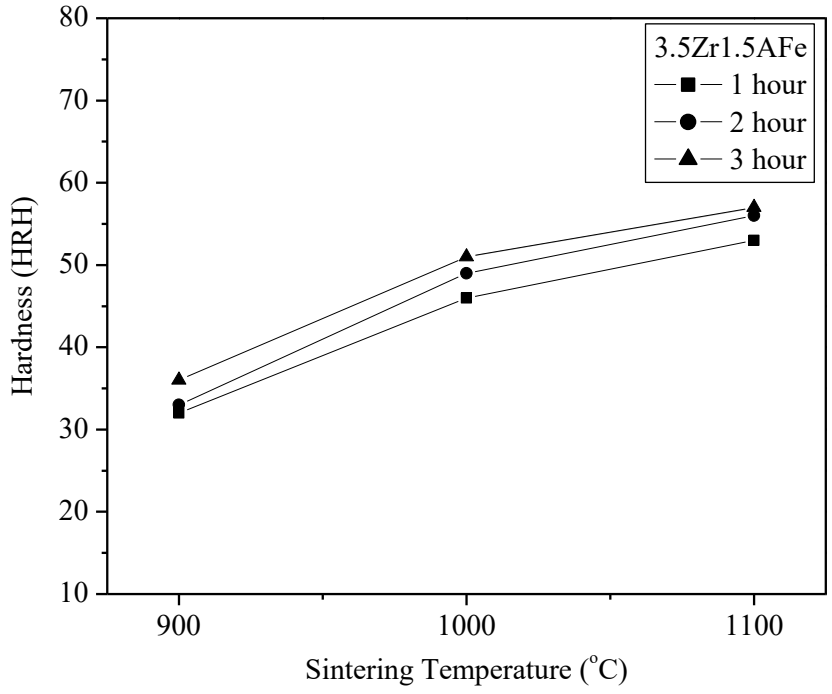

Fig. 8.33 Hardness vs. Sintering Temperature plots of various 3.5Zr1.5AFe specimens

The last slot of the specimens was sintered for 3 hour, specimen 3.5Zr1.5AFe900(3), 3.5Zr1.5AFe1000(3) and 3.5Zr1.5AFe1100(3) showed hardness number of 36 HRH, 51 HRH and 57 HRH. It can be concluded on the basis of the above discussion that the hardness values increases on increasing the sintering temperature as well as the time. Hardness number of the specimen was found to be dependent upon the iron aluminate as well as on the iron zirconate phase formation respectively. At high sintering temperature there was only a marginal difference in the hardness number values.

8.2.5 Wear

Specimens sintered at 900°C for 1,2 and 3 hour time interval were found to have low strength due to incomplete sintering and are not able to sustain frictional load during wear test. Therefore, the wear behavior of 900°C sintered specimens was not recorded. Fig. 8.34 and Table 8.4 shows the wear rate vs. load value for the specimen sintered at 1000°C. Specimen 3.5Zr1.5AFe1000(1) shows wear rate 0.5910 mm^3/km at a load of 0.5 kg, the same specimen showed wear rate 0.7650 mm^3/km at a load of 1.0 kg respectively. At a load of 1.5 kg and 2.0 kg the specimen showed wear rate 0.9651 mm^3/km and 1.2123 mm^3/km. On increasing the sintering time to 2 hour, the specimen 3.5Zr1.5AFe1000(2) showed wear rate 0.1273 mm^3/km at a load of 0.5 kg, 0.1762 mm^3/km at a load of 1.0 kg, 0.2637 mm^3/km at a load of 1.5 kg and 0.3841 mm^3/km at a load of 2.0 kg. Further increase in the sintering time to 3 hour yielded specimen 3.5Zr1.5AFe1000(3). At a load of 0.5 kg the specimen showed wear rate 0.1199 mm^3/km, at a load of 1.0 kg wear rate was found out to be 0.1396 mm^3/km, at a load of 1.5 kg the wear rate was 0.2167 mm^3/km and at a load of 2.0 kg the same specimen showed wear rate of 0.3113 mm^3/km.

In the similar manner Fig. 8.35 and Table 8.4 shows the wear rate vs. load and values of wear rate at different loads for the specimen sintered at 1000°C. Specimen 3.5Zr1.5AFe1100(1) shows wear rate of 0.1097 mm^3/km at a load of 0.5 kg, the same specimen showed wear rate of 0.1414 mm^3/km at a load of 1.0 kg respectively. At a

load of 1.5 kg and 2.0 kg the specimen showed wear rate of 0.2194 mm^3/km and 0.2710 mm^3/km. On increasing the sintering time to 2 hour specimen 3.5Zr1.5AFe1100(2) showed wear rate of 0.0888 mm^3/km at a load of 0.5 kg, 0.1212 mm^3/km at a load of 1.0 kg, 0.1653 mm^3/km at a load of 1.5 kg and 0.2222 mm^3/km at a load of 2.0 kg. Further increase in the sintering time to 3 hour yielded specimen 3.5Zr1.5AFe1100(3), at a load of 0.5 kg the specimen showed wear rate of 0.0436 mm^3/km, at a load of 1.0 kg wear rate was found out to be 0.0396 mm^3/km, at a load of 1.5 kg the wear rate was found out to be 0.0476 mm^3/km and at a load of 2.0 kg the same specimen showed wear rate of 0.0872 mm^3/km.

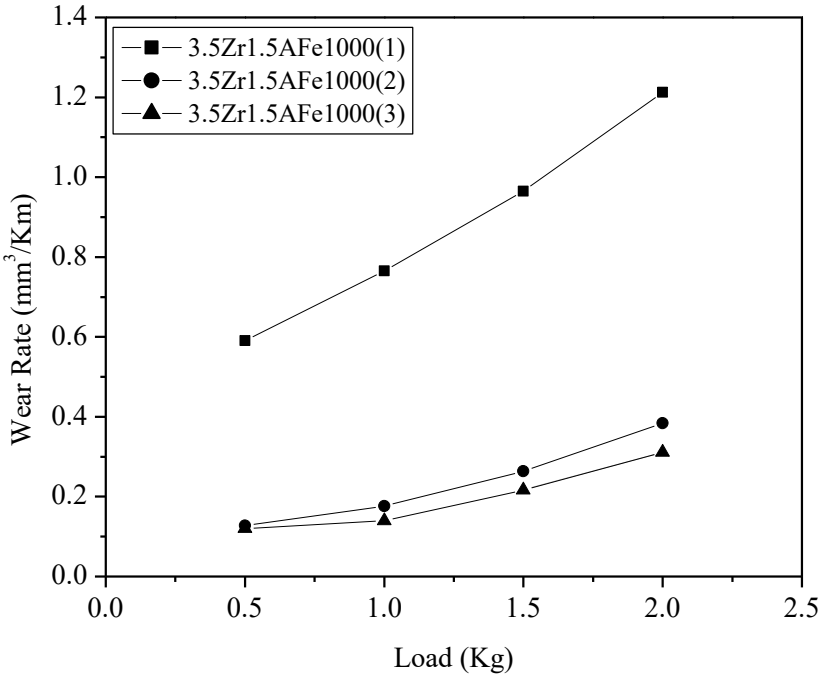

Fig. 8.34 Wear Rate vs. Load plots for specimen sintered at 1000°C

Table 8.4 Wear rate values of different 3.5Zr1.5AFe specimens at different loads

S. No.	Specimen Code	Wear Rate (mm^3/Km) at 0.5 Kg Load	Wear Rate (mm^3/Km) at 1.0 Kg Load	Wear Rate (mm^3/Km) at 1.5 Kg Load	Wear Rate (mm^3/Km) at 2.0 Kg Load
1.	3.5Zr1.5AFe1000(1)	0.5910	0.7650	0.9651	1.2123
2.	3.5Zr1.5AFe1000(2)	0.1273	0.1762	0.2637	0.3841
3.	3.5Zr1.5AFe1000(3)	0.1199	0.1396	0.2167	0.3113
4.	3.5Zr1.5AFe1100(1)	0.1097	0.1414	0.2194	0.2710
5.	3.5Zr1.5AFe1100(2)	0.0888	0.1212	0.1653	0.2222
6.	3.5Zr1.5AFe1100(3)	0.0436	0.0396	0.0476	0.0872

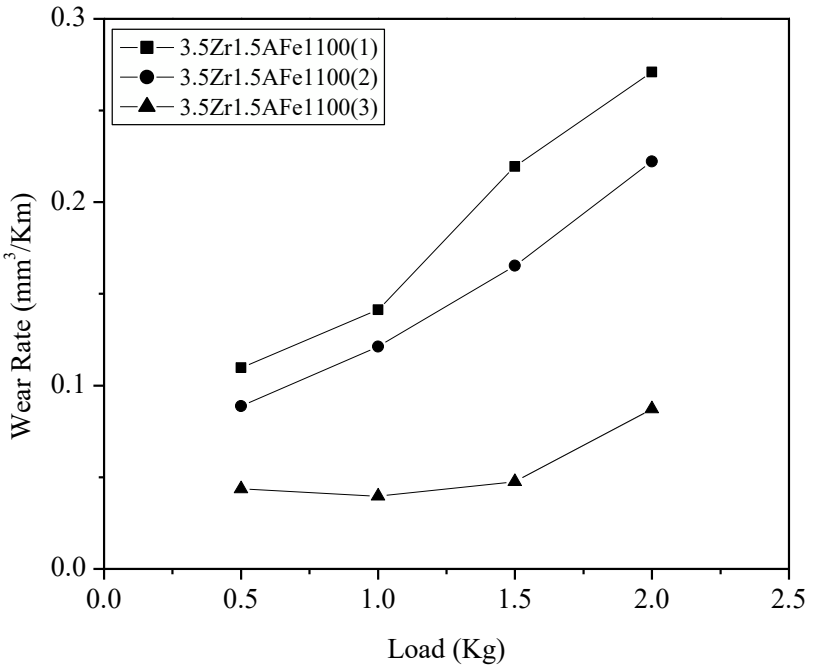

Fig. 8.35 Wear Rate vs. Load plots for specimen sintered at 1100°C

8.2.6 Scanning Electron Microscopy (After Wear)

Fig. 8.36 shows the microstructure of the weared specimen 3.5Zr1.5AFe1000(1) after 2.0 kg load at (a) 500X (b) 1000X and (c) 2000X magnification respectively. Fig. 8.36(a) shows the micrograph of the worn specimen at 500X which shows the light grooves generated over the entire surface of the specimen. The micrograph also shows some polishing marks on the specimen surface. Fig. 8.36(b) shows the micrograph of the worn specimen at 1000X which shows the removal of the material due to the presence of hard iron aluminate and iron zirconate phases. There is a tribofilm formation between the disc and the pin due to which there are scores on the specimen surface. Fig. 8.36(c) shows the micrograph of the worn specimen at 2000X which shows the removal of the material due to the adhesive wear. The wear rate generated on the specimen surface is extremely light and could not extend upto appreciable depth.

Fig. 8.37 shows the microstructure of the weared specimen 3.5Zr1.5AFe1000(2) after 2.0 kg load at (a) 500X (b) 1000X and (c) 2000X magnification respectively. Fig. 8.37(a) shows the micrograph of the worn specimen at 500X which shows the light grooves generated over the entire surface of the specimen. The micrograph also shows some polishing marks on the specimen surface. The grooves generated on the specimen surface are light in comparison to the specimen 3.5Zr1.5AFe1000(1). Fig. 8.37(b) shows the micrograph of the worn specimen at 1000X which shows the removal of the material due to the presence of hard iron aluminate and iron zirconate phase. There is a tribofilm formation between the disc and the pin due to which there are scores on the specimen surface. Fig. 8.37(c) shows the micrograph of the worn specimen at 2000X which shows the removal of the material due to the adhesive wear. There are some patches due to the microploughing on the specimen surface. The wear marks generated on the specimen surface is extremely light and could not extend upto appreciable depth.

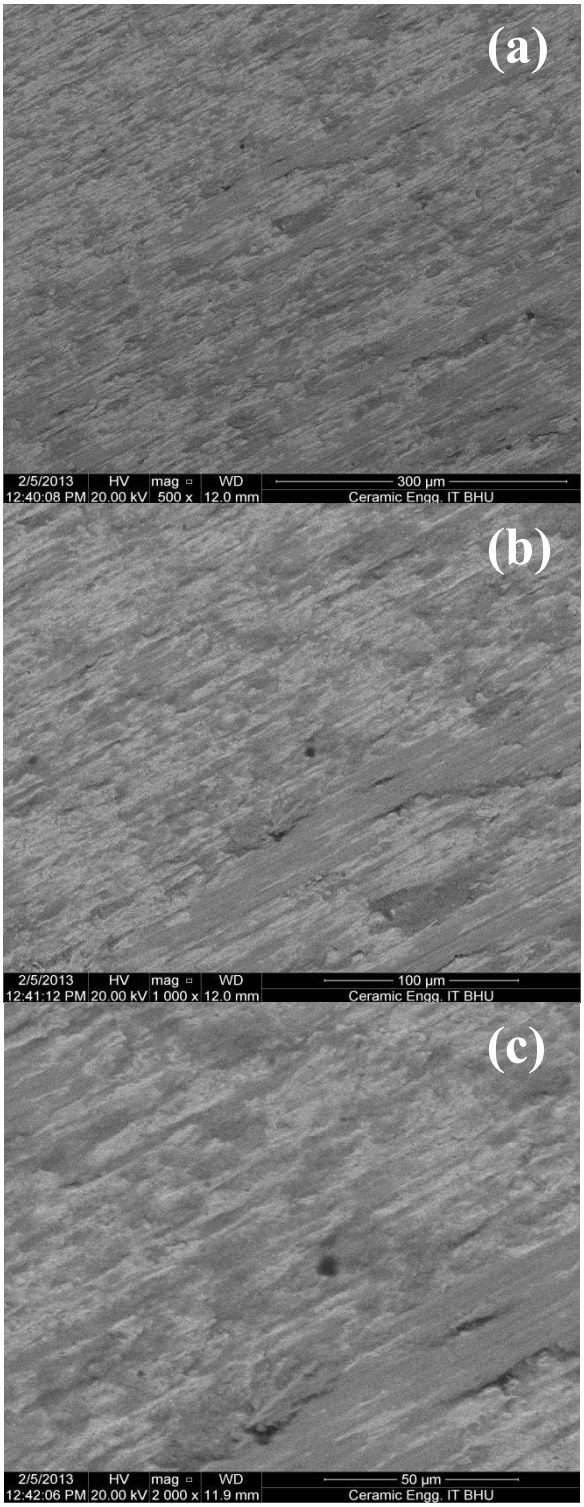

Fig. 8.36 Microstructure of worn specimen 3.5Zr1.5AFe1000(1) after 2.0 Kg load at (a) 500X (b) 1000X and (c) 2000 X magnification respectively

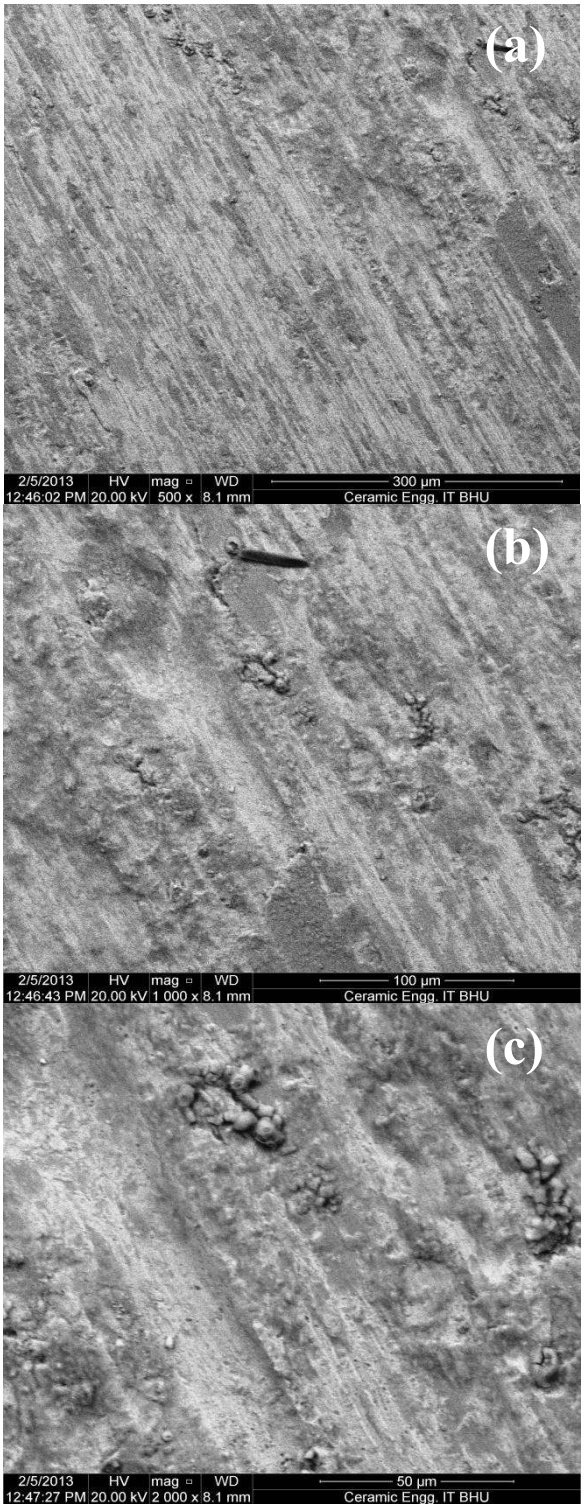

Fig. 8.37 Microstructure of the worn specimen 3.5Zr1.5AFe1000(2) after 2.0 Kg load at (a) 500X (b) 1000X and (c) 2000X magnification respectively

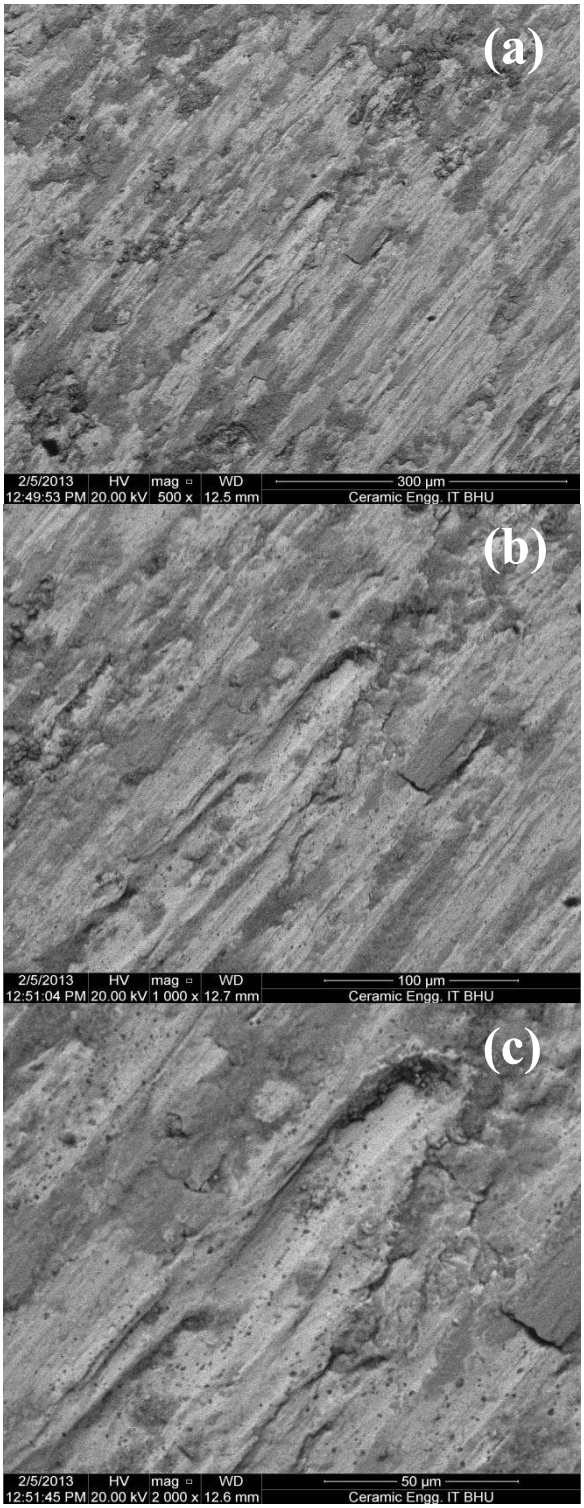

Fig. 8.38 Microstructure of the worn specimen 3.5Zr1.5AFe1100(2) after 2.0 Kg load at (a) 500X (b) 1000X and (c) 2000X magnification respectively

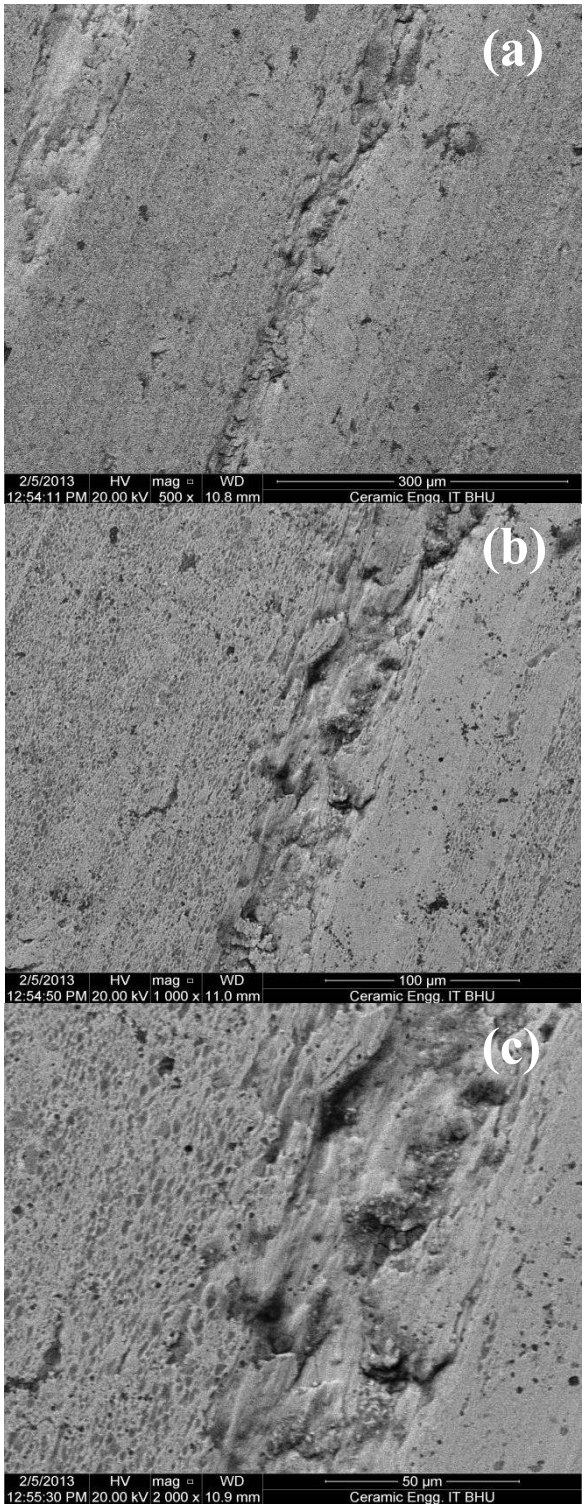

Fig. 8.39 Microstructure of the worn specimen 3.5Zr1.5AFe1100(3) after 2.0 Kg load at (a) 500X (b) 1000X and (c) 2000X magnification respectively

Fig. 8.38 shows the microstructure of weared specimen 3.5Zr1.5AFe1100(2) after 2.0 kg load at (a) 500X (b) 1000X and (c) 2000X magnification respectively. Fig. 8.38(a) shows the micrograph of the worn specimen at 500X which shows the light grooves along with some digging effect generated over the entire surface of the specimen. The present micrograph also shows some polishing marks on the specimen surface. The grooves generated on the specimen surface are light in comparison to the specimen 3.5Zr1.5AFe1000(1) and 3.5Zr1.5AFe1000(2). Fig. 8.38(b) shows the micrograph of the worn specimen at 1000X which shows the removal of the material due to the presence of hard iron aluminate and iron zirconate phase. There is a tribofilm formation between the disc and the pin due to which there are scores on the specimen surface. Fig. 8.38(c) shows the micrograph of the worn specimen at 2000X which shows the removal of the material due to the adhesive wear. There are some patches due to the fretting on the specimen surface. The wear marks which are generated on the specimen surface is extremely light and could not extend upto appreciable depth.

Fig. 8.39 shows the microstructure of weared specimen 3.5Zr1.5AFe1100(3) after 2.0 kg load at (a) 500X (b) 1000X and (c) 2000X magnification respectively. Fig. 8.39(a) shows the micrograph of the worn specimen at 500X which shows the light grooves along with some digging effect generated over the entire surface of the specimen. The present micrograph also shows some polishing marks on the specimen surface. The grooves generated on the specimen surface are light in comparison to the specimen 3.5Zr1.5AFe1000(1), 3.5Zr1.5AFe1000(2) and 3.5Zr1.5AFe1100(2). Fig. 8.39(b) shows the micrograph of the worn specimen at 1000X which shows the removal of the material due to the presence of hard iron aluminate and iron zirconate phase. There is a tribofilm formation between the disc and the pin due to which there are scores on the specimen surface. Fig. 8.39(c) shows the micrograph of the worn specimen at 2000X which shows the removal of the material due to the adhesive wear. There are some patches due to the fretting on the specimen surface. The wear marks which are generated on the specimen surface is extremely light and could not extend upto appreciable depth.

On the basis of the above discussion it can be concluded that in Fe-Al_2O_3-ZrO_2 hybrid metal matrix nanocomposites, consolidation and phase formation depends upon the sintering temperature and time respectively. At lower sintering temperature i.e. 900°C and sintering time of 1, 2 and 3h the reaction rate between the various particles is less due to which the amount of iron aluminate ($FeAl_2O_4$) and iron zirconium oxide (Zr_6Fe_3O) phase formation is reduced. Due to this reason the iron aluminate and iron zirconium oxide phases are detected in some specimen whereas it is not detected by the instrument in some specimen. At lower temperature and time of sintering, the specimen shows low density and hardness. However, on increasing the sintering temperature to 1000 and 1100°C for all time of sintering, more amount of iron aluminate and iron zirconate phases are formed. At higher temperature and time of sintering, the bonding between iron aluminate and iron zirconium oxide particles with the iron particles are improved. Due to the higher bonding strength the structural and mechanical properties is improved. Values of density and hardness are found to increase with an increase in the sintering temperature and time. Value of hardness for Fe-Al_2O_3, Fe-ZrO_2 metal matrix nanocomposites was found to be in the range of 40-45 HRH and 40-52 HRH whereas the hardness value of CoO doped Fe-Al_2O_3 nanocomposites were found to be in the range of 38-43 HRH. Hardness values [55-60 HRH] of the hybrid metal matrix nanocomposites were found to be better in comparison to the Fe-Al_2O_3, Fe-ZrO_2 and CoO doped Fe-Al_2O_3 metal matrix nanocomposites [Jha et al. (2013); Basavarajappa et al. (2007)]. Wear rate of the Fe-Al_2O_3 and CoO doped Fe-Al_2O_3 metal matrix nanocomposites was found to be high. Wear of the hybrid nanocomposite specimens was also found to be less as compared to Fe-Al_2O_3 and CoO doped Fe-Al_2O_3 metal matrix nanocomposites.

The next chapter presents a detailed study on the Corrosion behavior of Fe-Al_2O_3 metal matrix nanocomposites. Fe-5% Al_2O_3, Fe-10% Al_2O_3, CoO and CeO_2 doped Fe-Al_2O_3 metal matrix nanocomposites were synthesized and characterized using the Tafel polarization plots. XRD and SEM of the corroded specimens have also been carried out in order to study the effect of 1N HCl on the phase and morphology of the nanocomposite specimens.